EUROPEAN ORGANIZATION FOR NUCLEAR RESEARCH

CERN-PPE/91-50
13 March 1991

TESTS OF THE ELECTROWEAK THEORY AT THE Z RESONANCE

H. Burkhardt,
CERN, Geneva, Switzerland
and
Jack Steinberger,
CERN, Geneva, Switzerland, and Scuola Normale Superiore, Pisa, Italy

For Vol. 41 of the Annual Review of Nuclear and Particle Science

1 LEP

The Large Electron–Positron collider (LEP) at CERN came into operation in the summer of 1989 to produce its first Z's. The present center-of-mass energy is limited to 105 GeV. Energy upgrading is in progress, and the available energy is expected to exceed the W^+W^- pair production threshold of 160 GeV by at least 10 GeV, hopefully more, after 1994. LEP was conceived in the late seventies, following the prediction of the Z and $W^{\pm}$ by the new electroweak theory[1] which had been experimentally established by the discovery, in 1973[2], of the neutral current it had predicted. Perhaps the first suggestion for such a machine was that of Richter[3]. It was hoped that it might enable discovery of the Z, but fortunately for physics the Z as well as the W were found earlier, in $p\bar{p}$ collisions[4].

The design luminosity is 1.6×10^{31} cm^{-2} s^{-1} at the Z mass, and it has already been nearly (within a factor of 2) reached: in 1990 about three quarters of a million Z's were observed, hundreds of times more than had been seen in $p\bar{p}$ colliders, and under much cleaner conditions. The analysis of these Z decays is proceeding along several lines:

i) The study of the electroweak interaction at a higher energy and with higher precision than was possible before.
ii) Searches for new particles such as different varieties of Higgs bosons, supersymmetric particles, new quarks or leptons, excited leptons, and others.
iii) Studies of QCD in hadronic Z decay.
iv) Studies of heavy quarks, in particular the b quark, which is produced in interesting quantities in Z decay.

Substantial results in all four of these fields have already occasioned of the order of one hundred publications. Here we limit ourselves to the first topic, which has provided excellent evidence that there are just three fermion families, given an accurate value of the electroweak mixing angle through the precise measurement of the Z mass, and allowed substantially more precise checks on the electroweak theory than were possible previously, as well as, through its virtual effects, put limits on the mass of the top.

2 THE FOUR DETECTORS

Four of the eight collision points in LEP are equipped with detectors. These are constructed to measure the momenta of charged particles by magnetic tracking, and the energies of these as well as of neutral particles in electromagnetic followed by hadronic calorimeters, over as much of the 4π solid angle as possible. All four detectors emphasize the identification of electrons and muons. With respect to previous 4π detectors they present new levels of completeness of coverage, and precision in energy and angular measurement, especially in the calorimetry. The four collaborations each number several hundred physicists from dozens of institutions, distributed over the globe.

2.1 ALEPH

The ALEPH[5] detector is shown in Fig. 1. Tracking is done in three steps: a silicon strip microvertex chamber to reconstruct secondary vertices (this was not yet operational when the data reported here were taken), an inner drift chamber with an important event trigger function, and the main device, a 3.6 m diameter, 4.4 m long time projection chamber, which also furnishes ionization-density information for particle separation. The electromagnetic calorimeter is a 45 layer lead–proportional wire plane sandwich. The signal is read out from 72,000 three-storey towers which project to the collision zone,

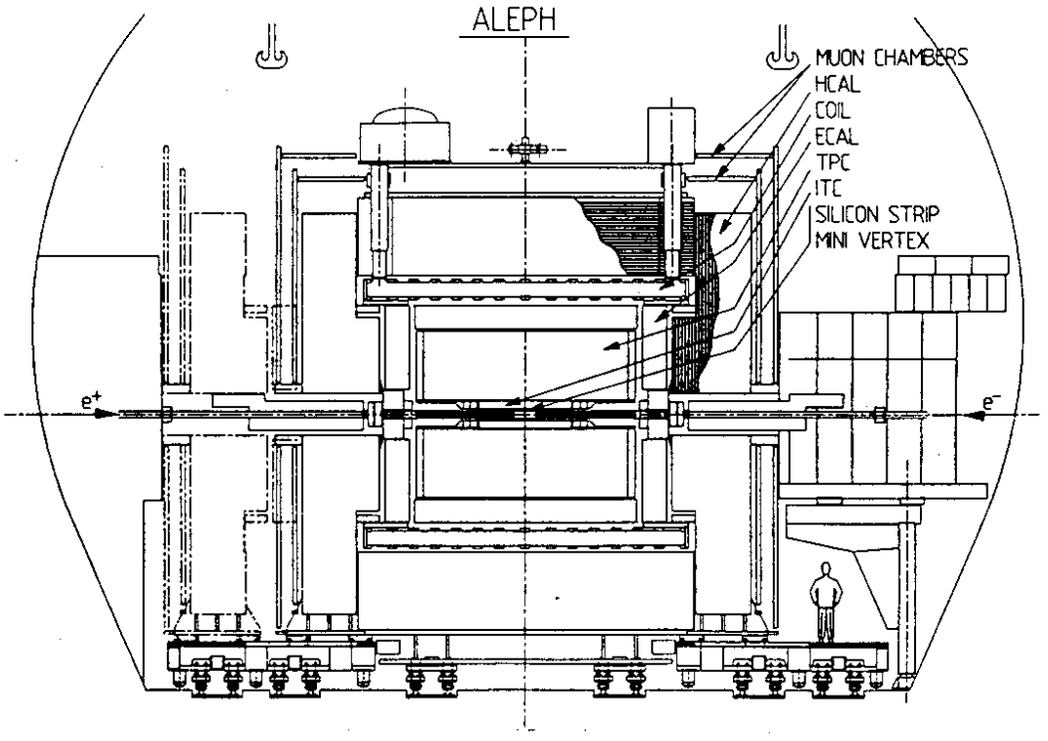

Fig. 1 The ALEPH detector.

as well as from each of the 45 wire planes in each of the 36 modules. Space resolution is $\sim 0.8° \times 0.8°$, energy resolution $0.19/\sqrt{E(\mathrm{GeV})} + 1.1\%$. The superconducting coil produces a field of 1.5 T. The return yoke serves as a hadron calorimeter. Sampling is by means of streamer tubes, every 5 cm of iron, with a total iron thickness of 1.2 m. The signal is read out in 4500 projective towers as well as on strips, every centimeter. The strip readout of the hadron calorimeter, together with two outer double layers of streamer tubes which are read out every 5 mm, serves to identify muons. A reconstructed Z decay into tau leptons is shown in Fig. 2. The main emphasis in ALEPH has been on

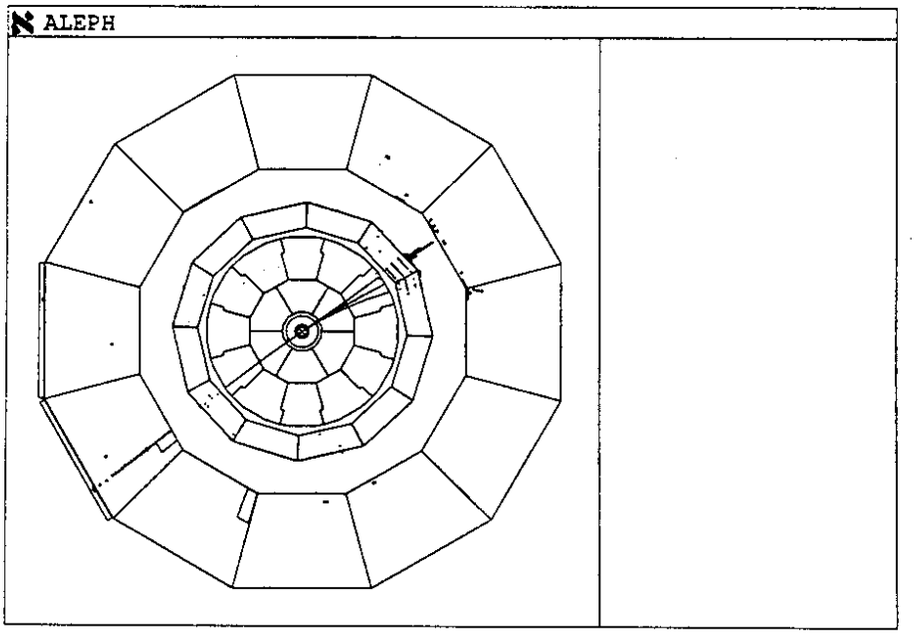

Fig. 2 An $e^+e^- \rightarrow \tau^+\tau^-$ event in ALEPH. The single track is due to the decay $\tau^- \rightarrow \mu^- + \nu_\mu + \nu_\tau$, the three-track decay to $\tau^+ \rightarrow 2\pi^+ + \pi^- + \nu_\tau$.

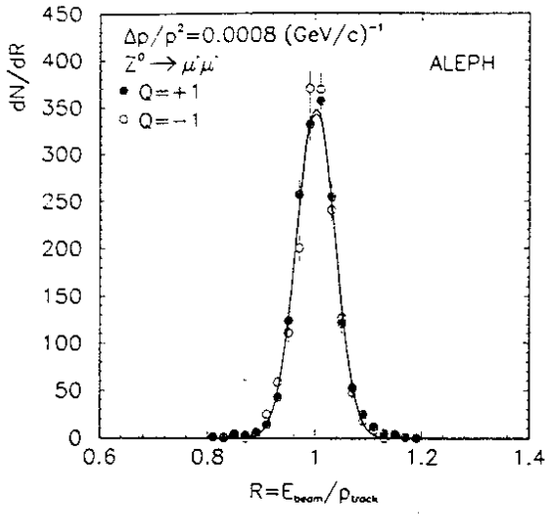

Fig. 3 ALEPH tracking resolution illustrated using the muonic Z decay; $\Delta p/p = 3.6\%$ at 45 GeV.

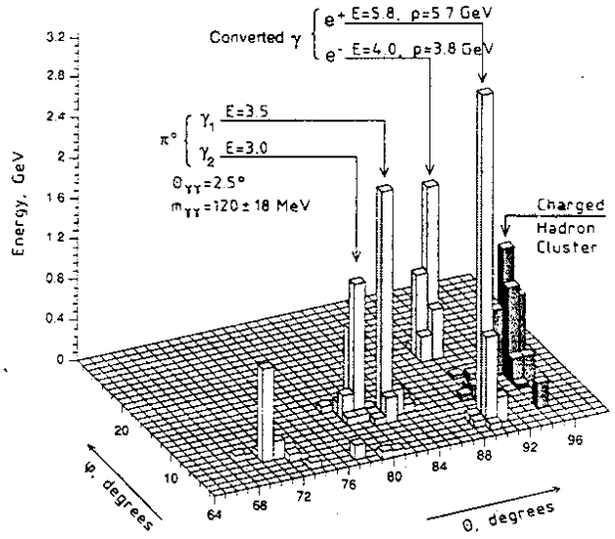

Fig. 4 Spatial resolution of the ALEPH electromagnetic calorimeter and its usefulness in the identification of electrons and photons. Part of a typical hadron jet is shown. Photons and electrons are identified by the lateral and longitudinal (not shown)
development of the shower. Electrons must have, in addition, an associated track
whose momentum matches the energy.

the precision of momentum measurement, with $\Delta p/p = 0.08\% \cdot p(\mathrm{GeV})$, corresponding to a resolution of 3.6% for 46 GeV muons (see Fig. 3), and also on the fine granularity of the electromagnetic calorimeter, essential in the identification of electrons as well as photons immersed in hadronic jets (see Fig. 4).

2.2 DELPHI

The DELPHI[6] detector is shown in Fig. 5. The inner tracking proceeds in three steps: a silicon microstrip detector to reconstruct secondary vertices, an inner jet drift chamber, and a time projection chamber, 2.4 m in diameter and 3 m in length, which also furnishes ionization-density information. A special feature of the DELPHI detector is the ring-imaging Cherenkov system, pioneered by that collaboration, and which, using both liquid and gas radiators, will permit e–π separation in the interval 0 to 4 GeV and π–K separation in the interval 0.5 to 7 and 9 to 25 GeV when it becomes fully operational (see

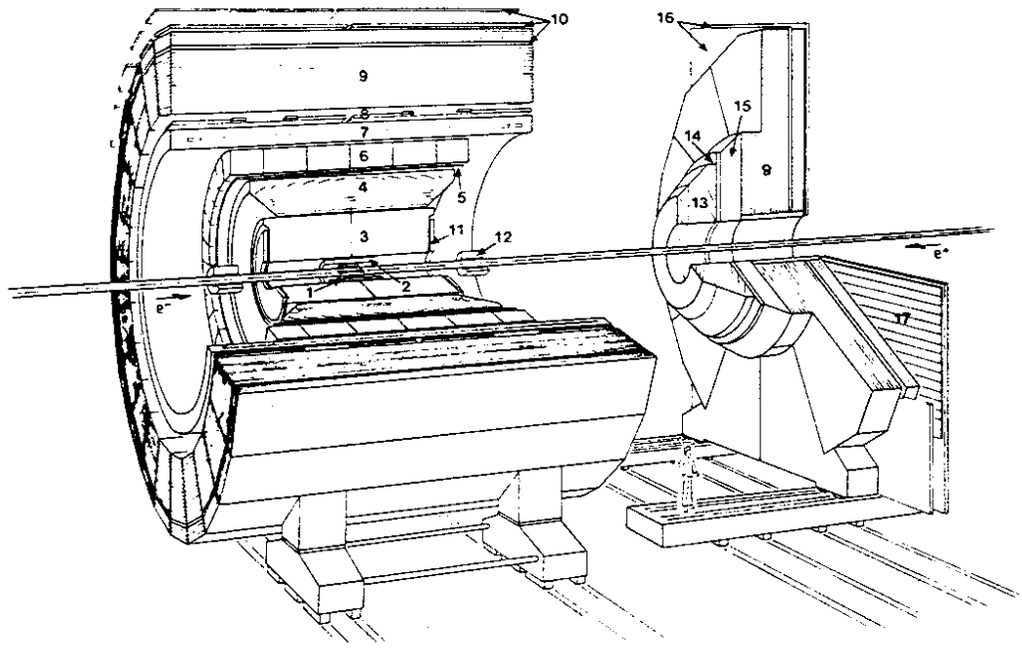

Fig. 5 The DELPHI detector. 1 = microvertex detector. 2 = inner detector. 3 = time projection chamber (TPC). 4 = barrel ring-imaging Cherenkov counter (RICH). 5 = outer detector. 6 = high-density projection chamber (HPC). 7 = superconducting solenoid. 8 = time-of-flight counters (TOF). 9 = hadron calorimeter. 10 = barrel muon chambers. 11 = forward chamber A. 12 = small-angle tagger (SAT) = luminosity monitor. 13 = forward RICH. 14 = forward chamber B. 15 = forward electromagnetic calorimeter. 16 = forward muon chambers. 17 = forward scintillator hodoscope.

Fig. 6). There follows an outer tracking of 5 layers of drift tubes. The momentum resolution achieved for the muons from Z decay is 7%. The barrel electromagnetic calorimeter is a heavy projection chamber, in which the ionization produced in the gas between lead layers is drifted to the ends of the 90 cm long modules. This technique also has been pioneered by DELPHI and offers excellent spatial resolution. The superconducting coil produces a field of 1.2 T. It is surrounded by a scintillator hodoscope for time-of-flight information. The return yoke is instrumented as a hadron calorimeter with streamer tube layers every 5 cm of iron, for a total iron thickness of 1 m. The signals are read out in ~ 4000 projective towers. The whole set-up is surrounded by three layers of muon detectors. An exceptional hadronic event is shown in Fig. 7.

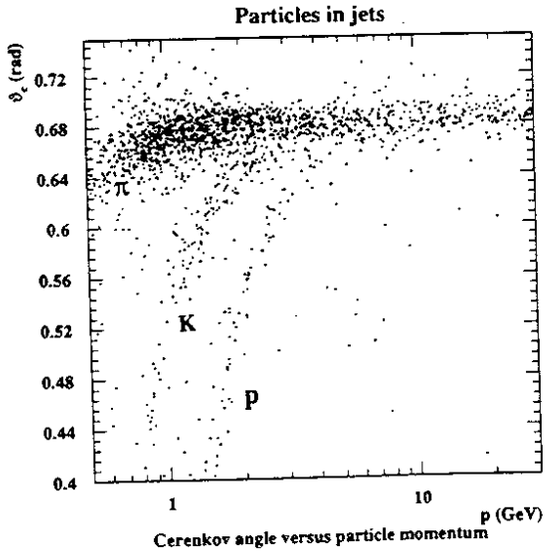

Fig. 6 Particle separation in the DELPHI barrel ring-imaging Cherenkov counter, liquid part.

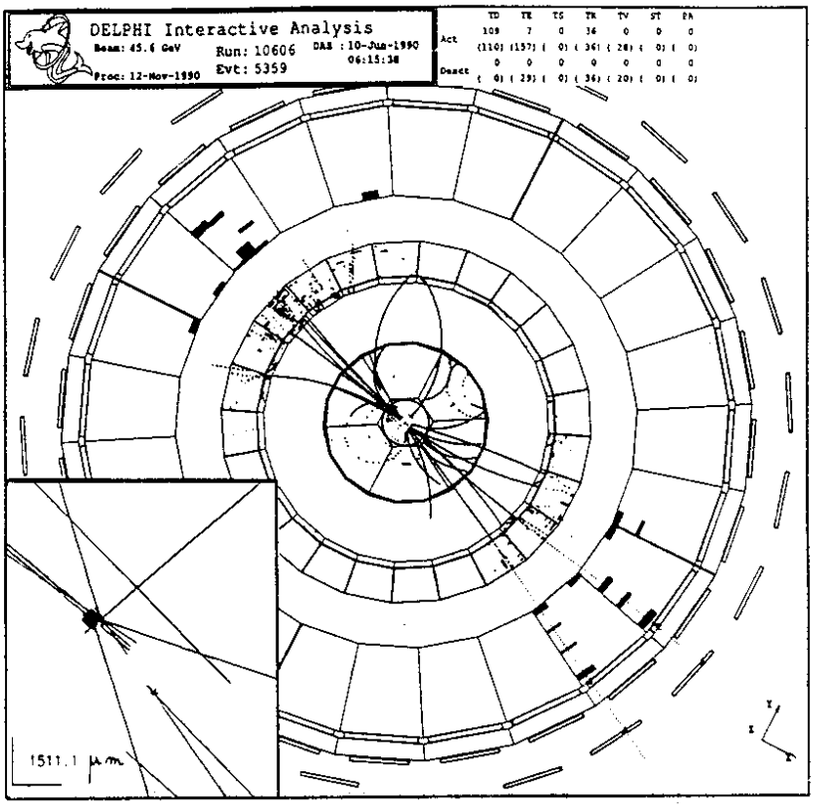

Fig. 7 Rare hadronic Z decay in DELPHI. The inset shows the decay of a neutral particle after a trajectory of 1.5 mm, on the basis of the very precise silicon strip measurements. The two secondaries are identified as muons. From their momenta and included angles, it is identified as a J/ψ, probably from B decay.

2.3 L3

The L3 detector[7] is shown in Fig. 8. It is remarkable in its sheer physical size, and in the fact that the general tracking is minimized in favor of precise outer tracking for muons only. The central tracking chamber is a jet-type time expansion chamber with 18 cm inner diameter, 80 cm outer diameter, and 105 cm length, designed to measure

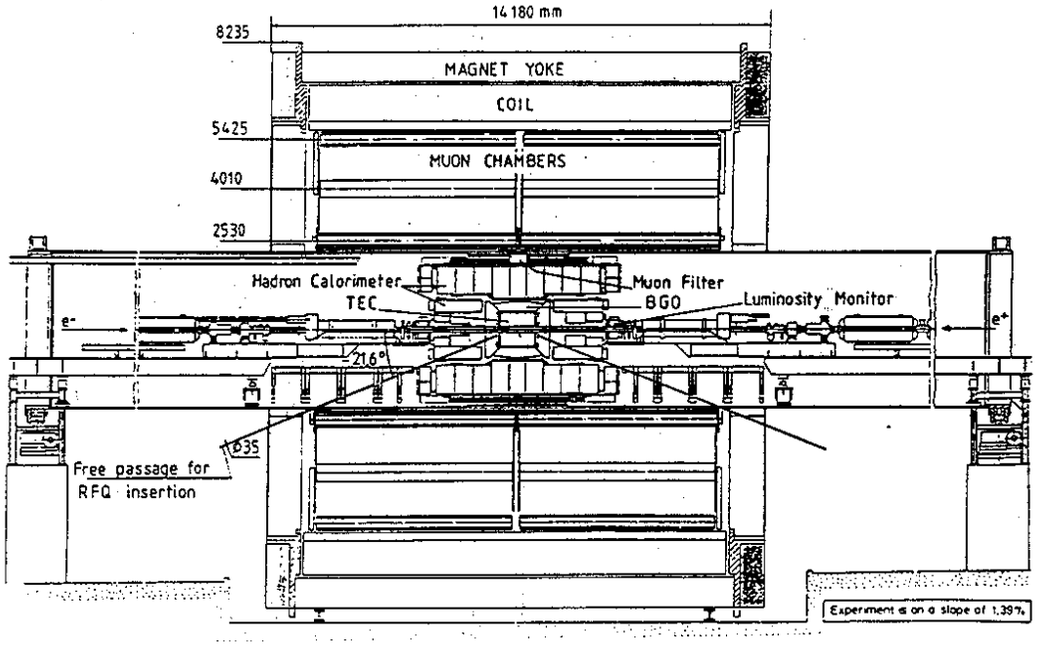

Fig. 8 The L3 detector.

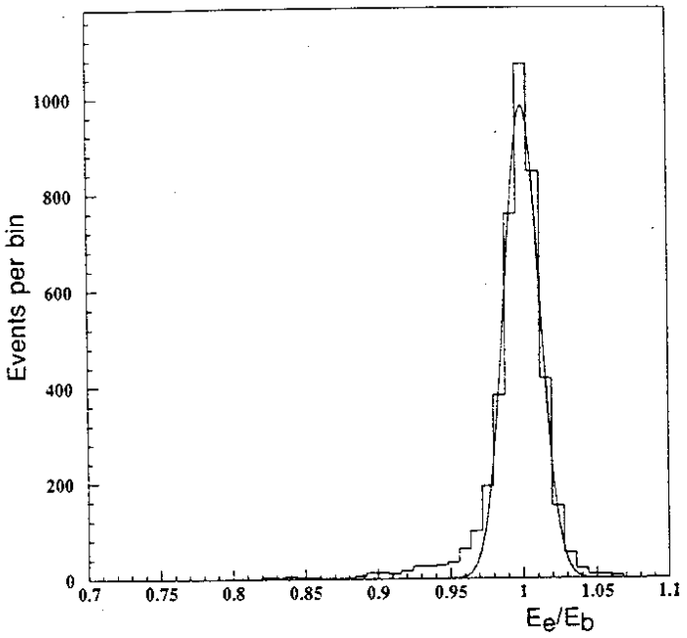

Fig. 9 The energy resolution observed in the L3 electromagnetic calorimeter for electrons of Bhabha events, $\sigma(E_e)/E_{\rm beam}$ is 1.4%.

the direction and the sign of the electric charge of charged particles up to 50 GeV. The electromagnetic calorimeter is constructed of 10,752 bismuth germanium oxide scintillator prisms, corresponding to an angular resolution of $2° \times 2°$. The energy resolution is exceptional, particularly at low energy. At 45 GeV it is 1.4%, entirely limited by systematics (see Fig. 9). For the results reported here, the barrel part was in place, but not the two end-caps. The hadron calorimeter is a 58 layer uranium–proportional wire plane sandwich, arranged in 144 modules, read out on the wires with a high granularity. The momenta of the penetrating muons in the polar angle interval 40°–140° are measured with high precision in the very large (inner diameter = 4.8 m, outer diameter = 11 m) solenoidal magnet with a field of 0.5 T. The momentum resolution for the 45 GeV muons of Z decay is 2.2 to 3%. A hadronic event is shown in Fig. 10.

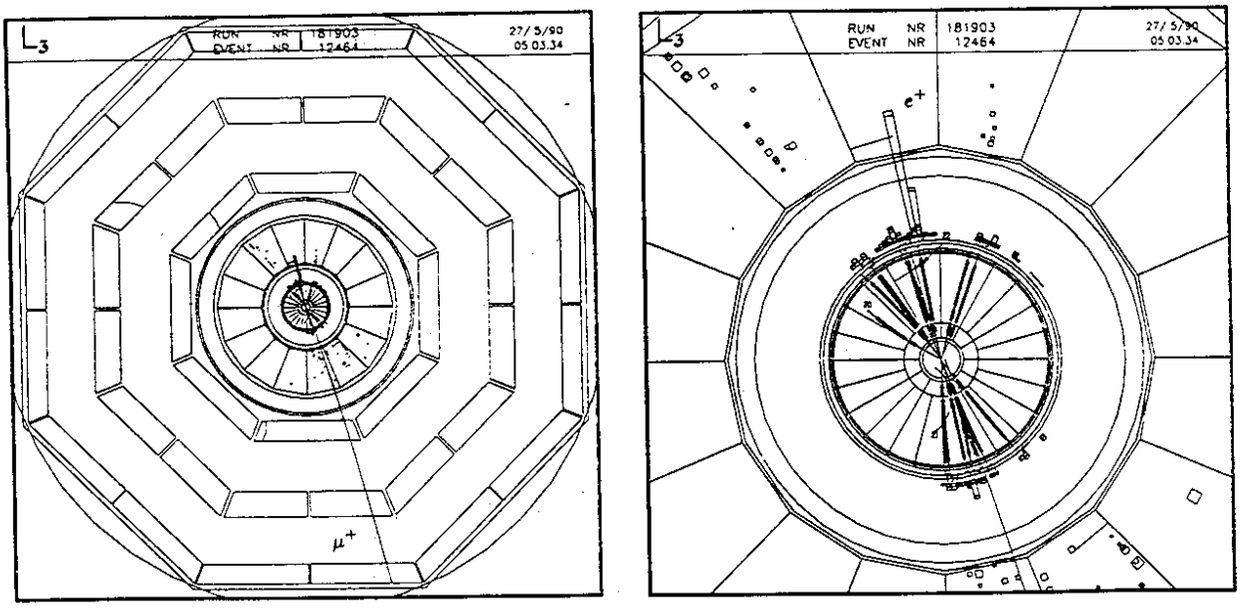

Fig. 10 Hadronic Z decay in L3 with muon.

2.4 OPAL

The OPAL detector[8] is shown in Fig. 11. Tracking is by means of jet-type drift chambers, at a pressure of 4 atm, to gain in both space and ionization-density resolution. The inner 'vertex' part covers the radial interval between 9 and 22 cm and is 1 m long; the outer, main chamber has an outer diameter of 3.7 m and is 4 m long. There are altogether 177 wires in the combined radial interval. The jet chamber is surrounded by a layer of chambers which drift the ionization along the z direction, in order to measure the z coordinates with higher precision than possible by the charge division used in the jet chamber. The warm solenoid provides the axial field of 0.44 T. The momentum resolution for 45 GeV muons is 6.8%. A layer of scintillation counters is used to measure the time of flight and in the trigger. An electromagnetic 'presampler', a double layer of streamer tubes, is used to measure the positions of photons and electrons which have showered in the 2 radiation lengths of the coil. The electromagnetic calorimeter is made of 11,700 projective

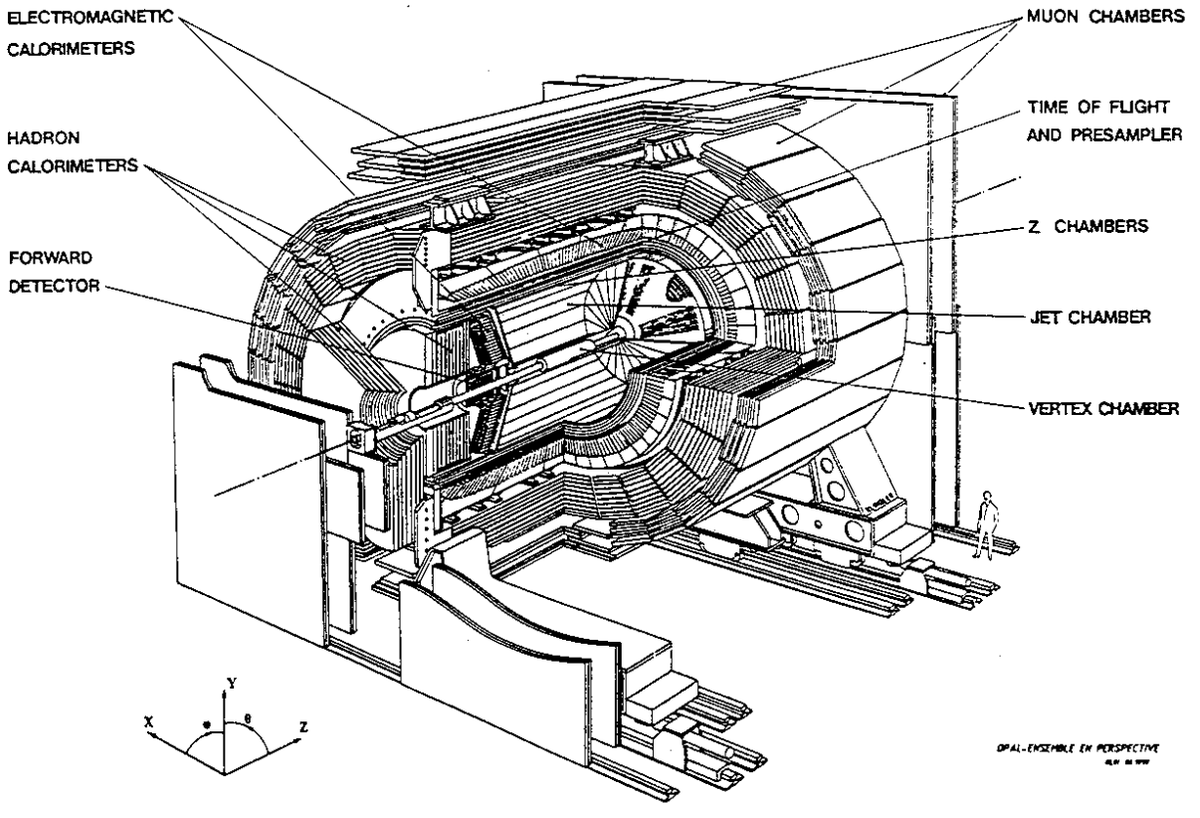

Fig. 11 The OPAL detector.

lead-glass blocks, corresponding to a granularity of 1.9° × 1.9°. Energy resolution is 3% for 45 GeV electrons. The return yoke consists of eight 10 cm slabs of iron, with layers of streamer tubes in between, serving as a hadron calorimeter. These are read out in 976 projective towers and on strips every centimeter. The whole apparatus is surrounded by four layers of muon detectors. Figure 12 shows a typical hadronic event. One of the great successes of OPAL is the tracking precision. Figure 13 illustrates the precision achieved in reconstructing the impact parameter of a track near the vertex, using the muons of Z decay as an example. The result, 40 μm, is truly excellent. Figure 14 shows the particle separation obtained in the ionization measurement.

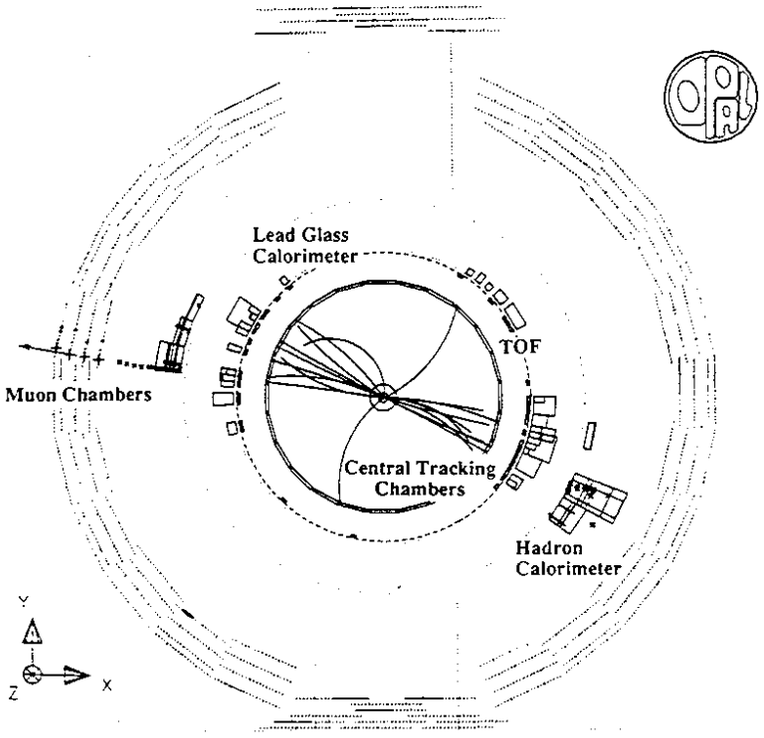

Fig. 12 Hadronic Z decay in OPAL.

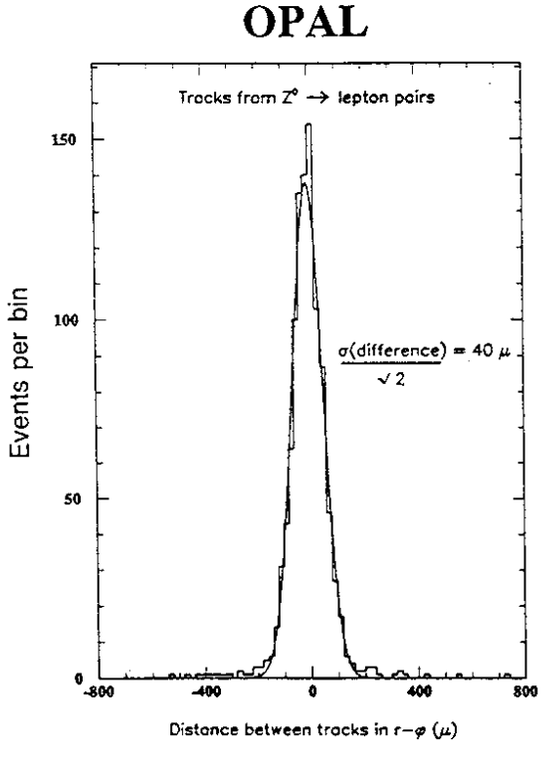

Fig. 13 Illustration of the precision of track reconstruction in OPAL: the distance between the two tracks of muonic Z decay, at the vertex. The error in the impact parameter is 40 μm.

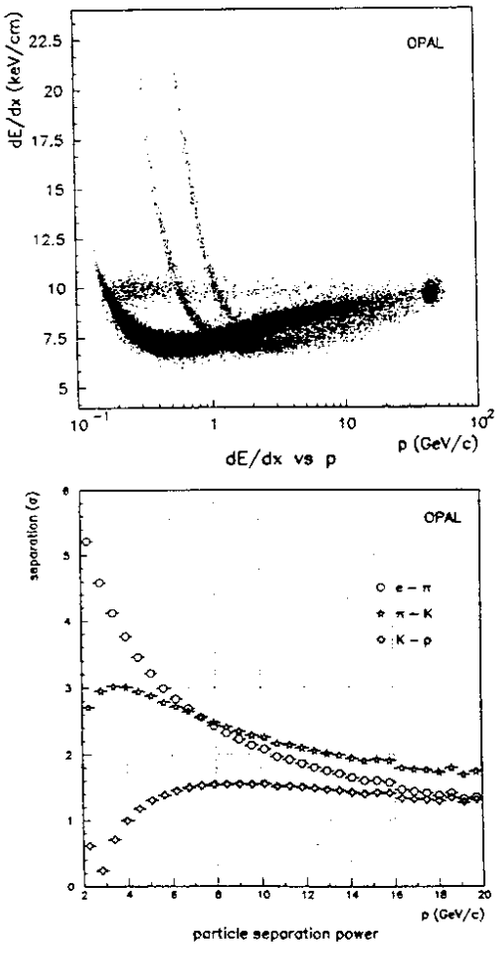

Fig. 14 Ionization density measurement in OPAL and its usefulness in particle identification.

3 PHYSICS AT THE Z RESONANCE

The center-of-mass energy available at LEP, 105 GeV at present, is clearly much less than the 2000 GeV at the Tevatron $p\bar{p}$ collider, even after allowance is made for the fact that the quark–antiquark center-of-mass energy is only a fraction of the $p\bar{p}$ energy. The strength of the e^+e^- collider is the simplicity of the initial state which is carried over to the final state, so that, in general, the rates for different channels can be calculated in the frame of present theories, and can be experimentally sorted out (except that the different quark-flavor channels can only rarely be identified).

At collision energies near the Z mass, the cross-section is enhanced through the Breit–Wigner resonance denominator by a factor of the order of $(m_Z/\Gamma_Z)^2 \sim 10^3$. Since the non-resonant cross-section is very small, of the order of $4\alpha^2/s$, the resonance presents a very important experimental opportunity, by its magnitude alone. All the work at LEP up to now has been on or near the Z peak for this reason.

3.1 Model-independent analysis of the Z line shape

The cross-section studies we discuss here are processes in which, in Born approximation, either a photon or a Z is exchanged, and a fermion pair is emitted:

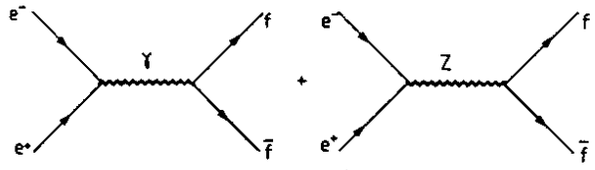

The fermion f may be: a charged lepton e, μ, or τ; a neutrino ν_e, ν_μ, or ν_τ; or one of five quark flavors u, d, s, c, or b. No novel channels have been observed.

The energy dependence of Z production is described by a relativistic Breit–Wigner line shape, which, however, must be corrected for initial-state radiation[9]:

$$\sigma_f(s) = \frac{12\pi\Gamma_e\Gamma_f}{m_Z^2} \frac{s}{|s - m_Z^2 + i\, s\Gamma_Z/m_Z|^2} [1 + \delta_{\rm rad}(s)] \,. \qquad (1)$$

Here m_Z is the Z mass, Γ_e, Γ_f are the Z partial decay widths to the electron and final-state fermion respectively, $s = E_{\rm cm}^2$, the square of the center-of-mass energy, and $\delta_{\rm rad}(s)$ is the effect of the initial-state radiation correction. In Eq. (1) the contribution of small terms due to photon exchange and its interference with Z exchange have been omitted for clarity. In the analysis of the experimental results these terms are, however, always included. The correction for the initial-state radiation, $\delta_{\rm rad}(s)$, is large, as can be seen in Fig. 15. It

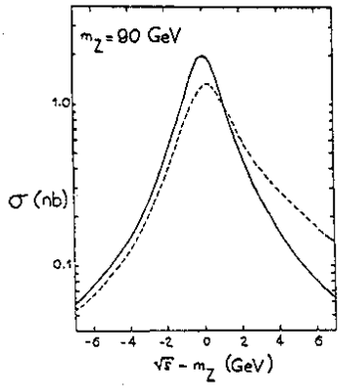

Fig. 15 Z line shape without and with initial-state radiative correction.

is 40% on the Z peak, but is known with a precision adequate for the present levels of experimental accuracy. Fits of expression (1) to the experimental line shapes of the different channels furnish model-independent values for m_Z, Γ_Z, Γ_f, and σ_f^{peak}, where σ_f^{peak} is defined as the cross-section at the peak of the resonance for channel f after unfolding the initial-state radiation:

$$\sigma_f^{peak} = \frac{12\pi}{m_Z^2}\frac{\Gamma_e\Gamma_f}{\Gamma_Z^2} . \tag{2}$$

3.2 Electroweak Born approximation and radiative corrections

The three parameters of the electroweak theory can be fixed at low energies through measurements of the electromagnetic fine structure constant α, the Fermi constant G_F obtained from the muon lifetime, and the weak mixing angle $\sin^2\theta_w$ obtained in the measurement of the ratio of charged- to neutral-current cross-sections in neutrino scattering. The masses of the fermions and of the Higgs particle are not predicted by the theory and can be considered as additional parameters. The masses of the $W^\pm$ and Z are instead directly related to the three coupling parameters of the theory through

$$\frac{m_W^2}{m_Z^2} = \cos^2\theta_w \tag{3}$$

and

$$\frac{\pi\alpha}{\sqrt{2}G_F} = m_Z^2\cos^2\theta_w\sin^2\theta_w = A_0^2 = (37.2802 \pm 0.0003\ \text{GeV})^2. \tag{4}$$

In Born approximation the differential cross-section for the reaction $e^+e^- \to f\bar{f}$ is

$$\frac{d\sigma_t}{d\Omega} = \frac{\alpha^2 N_c^f}{4s}\{F_1(s)(1+\cos^2\theta) + 2F_2(s)\cos\theta\} . \tag{5}$$

Here

θ is the center-of-mass production angle,
N_c^f is the colour factor, 3 for quarks, otherwise 1,
$F_1(s) = Q_f^2 - 2v_e v_f Q_f \mathrm{Re}\ \chi + (v_e^2+a_e^2)(v_f^2+a_f^2)|\chi|^2$,
$F_2(s) = -2a_e a_f Q_f \mathrm{Re}\ \chi + 4v_e a_e v_f a_f |\chi|^2$,
Q_f is the electric charge in units of the charge of the positron,
$\chi = s/(s - m_Z^2 + im_Z\Gamma_Z)$ is the Breit–Wigner resonance denominator,
$v_f = (I_3^f - 2Q_f\sin^2\theta_w)/(2\sin\theta_w\cos\theta_w)$ is the weak vector coupling constant,
$a_f = I_3^f/(2\sin\theta_w\cos\theta_w)$ is the weak axial-vector coupling constant,
I_3 is the third component of weak isospin, and
$\Gamma_Z = \Sigma_f\Gamma_f$ is the total width of the Z.

The first term in F_1 is pure photon exchange, the last term is pure Z exchange, and the central term is the interference between the two.

The integrated cross-section at and near the peak is dominated by the Z exchange, $|\chi|^2$ term:

$$\sigma_f = N_c^f\frac{4\pi}{3}\frac{\alpha^2}{s}(v_e^2+a_e^2)(v_f^2+a_f^2)|\chi|^2. \tag{6}$$

Since the partial widths are:

$$\Gamma_f = \frac{N_c^f}{3}\,\alpha\, m_Z(v_f^2+a_f^2)\,, \tag{7}$$

the Born approximation cross-section (5), when integrated over the solid angle, near the Z pole, has the Breit–Wigner form for spin 1 exchange:

$$\sigma = \frac{12\pi\Gamma_e\Gamma_f}{m_Z^2}\,\frac{s}{|s - m_Z^2 + i\, m_Z\Gamma_Z|^2}\,. \tag{8}$$

The Born approximation is not adequate for the analysis of the LEP experiments; it is essential to include higher-order radiative corrections. These include initial-state photon, and final-state photon and gluon radiation corrections, vertex and propagator corrections, and other even smaller corrections. They have been very much studied, and a summary of information and references to other papers are given in the Proceedings of the 1989 CERN Workshop on Z Physics at LEP 1 [10]. The initial-state radiation can be factored out as shown in expression (1).

The other corrections are small and calculable in the Standard Model. However, they depend on the unknown Higgs and top masses, as well as on the value of the strong coupling constant α_s, which is not yet very precisely known. The *dominant* effects of these corrections can be summarized by replacing $\sin^2\theta_w$ by an 'effective mixing angle' $\overline{\sin^2\theta_w}$ at the Z mass, by replacing α by its renormalized value at the Z mass:

$$\alpha(m_Z^2) = \frac{\alpha}{1 - \Delta\alpha} = 1.064\alpha \quad ,$$

by inserting the factor $\rho = 1/(1 - \Delta\rho)$ in the relationships between m_W and m_Z and between G_F and m_Z:

$$\frac{m_W^2}{m_Z^2} = \rho\,\overline{\cos^2\theta_w} \tag{9}$$

$$\frac{\pi\alpha(m_Z^2)}{\sqrt{2}G_F} = \rho\, m_Z^2\,\overline{\sin^2\theta_w}\;\overline{\cos^2\theta_w}\;, \tag{10}$$

with

$$\begin{aligned}\Delta\rho &\simeq 3G_F m_t^2/8\sqrt{2}\pi^2 - 11G_F m_Z^2 \sin^2\theta_w\, \ln(m_H/m_W)/12\pi^2\sqrt{2} \\ &= 0.0026 m_t^2/m_Z^2 - 0.0015\, \ln(m_H/m_W)\;,\end{aligned}$$

and, for the quark channels, including the second-order QCD correction, by replacing N^f by[11]

$$N_c^f(1 + \alpha_s/\pi + 1.4\alpha_s^2/\pi^2) \quad . \tag{11}$$

Finally, χ in Eq. (5) should be replaced by

$$\chi = \frac{s}{(s - m_Z^2) + i\, s\Gamma_Z/m_Z} \quad . \tag{12}$$

These changes give the major radiative corrections for all channels $e^+e^- \to f\bar{f}$ [12], except the $b\bar{b}$ channel, which requires an additional term that takes into account relatively large t–b amplitudes in the vertex corrections. To give some feeling for the magnitude of the corrections, the top mass, Higgs mass, and α_s dependences of Γ_ℓ, Γ_b, and Γ_Z are shown in Fig. 16.

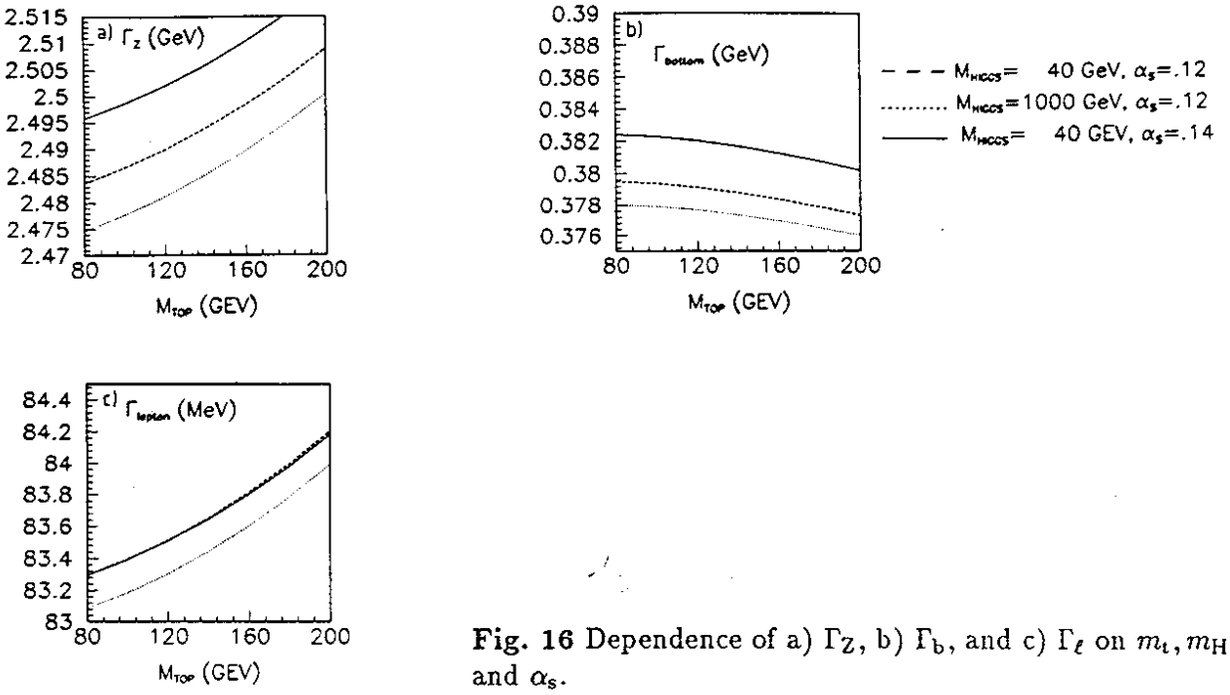

Fig. 16 Dependence of a) Γ_Z, b) Γ_b, and c) Γ_ℓ on m_t, m_H, and α_s.

3.3 Asymmetries

The forward–backward asymmetry in the angular distribution (5), as well as the polarization asymmetries, measure the vector–axial-vector coupling ratios for the different channels.

3.3.1 Forward–backward asymmetries A_{FB}

The forward–backward asymmetry A_{FB} is defined as the difference between forward and backward cross-sections divided by their sum:

$$A_{FB}^f = \frac{\int_0^1 (d\sigma_f/d\cos\theta) d\cos\theta - \int_{-1}^0 (d\sigma_f/d\cos\theta) d\cos\theta}{\int_0^1 (d\sigma_f/d\cos\theta) d\cos\theta + \int_{-1}^0 (d\sigma_f/d\cos\theta) d\cos\theta} .$$

From Eq. (5), $A_{FB} = \frac{3}{4} F_2/F_1$. Above and below the Z peak, the asymmetry is dominated by the interference term in F_2,

$$A_{FB}^f \simeq \frac{3}{2} \frac{a_e a_f Q_f \, \mathrm{Re}\, \chi}{(v_e^2 + a_e^2)(v_f^2 + a_f^2)} .$$

but exactly on the peak this term vanishes, and

$$A_{FB}^f = 3 \frac{v_e a_e v_f a_f}{(v_e^2 + a_e^2)(v_f^2 + a_f^2)} . \qquad (13)$$

For leptons, $v_\ell/a_\ell = 1 - 4\sin^2\theta_w$ is very small, leading to the small asymmetry at the peak $A_{FB}^{\ell,\mathrm{peak}} \simeq 3(v_\ell/a_\ell)^2$. This asymmetry at the peak furnishes a direct measure of v_ℓ/a_ℓ, but the sensitivity is compromised by the smallness of v_ℓ/a_ℓ together with the quadratic dependence.

For quarks,

$$A_{FB}^q = 3 \frac{v_e}{a_e} \frac{v_q}{a_q(1 + v_q^2/a_q^2)} ,$$

where

$$v_q/a_q = 1 - \tfrac{8}{3}\sin^2\theta_w \text{ for up-type quarks,}$$

and

$$v_q/a_q = 1 - \tfrac{4}{3}\sin^2\theta_w \text{ for down-type quarks.}$$

In contrast to leptons, v_q/a_q is not very small compared to one. This itself would facilitate the measurement of v/a in the quark asymmetries, but at least at the present technical level, this advantage is outweighed by the difficulty of separating the individual quark channels and identifying the quark jet relative to the antiquark jet in hadronic decays.

3.3.2 Polarization asymmetries

We consider here the case where the polarization of one of the four particles is measured. The case where this is the incident electron or positron is potentially very interesting, but this is not yet possible at LEP.

At present the only possibility is offered by the τ, which can sign its polarization in its decay. The polarization dependence of the cross-section is

$$\frac{d\sigma}{d\cos\theta}(\cos\theta, p) \propto (1+\cos^2\theta)F_1(s) + 2\cos\theta F_2(s) + p[(1+\cos^2\theta)F_3(s) + 2\cos\theta F_4(s)], \quad (14)$$

where p is the helicity of the τ.

At the Z pole:

$$\begin{aligned} F_1(m_Z^2) &= (v_e^2 + a_e^2)(v_f^2 + a_f^2) \\ F_2(m_Z^2) &= 4v_e a_e v_f a_f \\ F_3(m_Z^2) &= 2(v_e^2 + a_e^2) v_f a_f \\ F_4(m_Z^2) &= 2v_e a_e (v_f^2 + a_f^2). \end{aligned}$$

The polarization asymmetry A_{pol} is defined by

$$\begin{aligned} A_{pol} &= \langle p \rangle \equiv -\frac{\sigma_{p=1} - \sigma_{p=-1}}{\sigma_{p=1} + \sigma_{p=-1}} = -\frac{F_3}{F_1} \\ &= -\frac{2v_f a_f}{v_f^2 + a_f^2} \quad , \end{aligned} \quad (15)$$

and the forward–backward polarization asymmetry A_{pol}^{FB} is defined by

$$A_{pol}^{FB} \equiv$$

$$\frac{\int_0^1 d\cos\theta[d\sigma_{p=1}/d\cos\theta - d\sigma_{p=-1}/d\cos\theta] - \int_{-1}^0 d\cos\theta[d\sigma_{p=1}/d\cos\theta - d\sigma_{p=-1}/d\cos\theta]}{\int_{-1}^1 d\cos\theta[d\sigma_{p=1}/d\cos\theta + d\sigma_{p=-1}/d\cos\theta]}$$

$$= -\frac{3}{4}\frac{F_4}{F_1} = -3/4\frac{2v_e a_e}{v_e^2 + a_e^2} \, . \quad (16)$$

4 CROSS-SECTIONS AT THE Z PEAK

The experimental results reviewed here are the cross-sections for the four channels: $q\bar{q}$, e^+e^-, $\mu^+\mu^-$, and $\tau^+\tau^-$, as a function of the center-of-mass energy, production angle and, in the case of the τ, its polarization. The aims are the measurement of the Z mass, the check of predictions of the electroweak theory, and the detection of effects of the top and/or Higgs in the small radiative corrections. Since there are now nearly one million Z decays, and many more are expected, systematic precision at a level well below 1% becomes necessary. This enters in the triggering of events, their selection and acceptance, the measurement of the luminosities, and in the calibration of the beam energy. During this first period, LEP was operated in cycles lasting about one week; about one half of

the luminosity of each cycle was devoted to the energy of the Z peak; the rest was divided roughly equally among the six energies, $\pm 1, \pm 2$, and ± 3 GeV from the peak energy, for a total luminosity of ~ 10 pb^{-1}. The data-taking efficiencies of the four experiments varied between 60 and 80%.

In the following discussions on triggering, event selection, acceptance, and luminosity determination, it would be too lengthy and tedious to give the details for any, much less all four, of the experiments. We limit ourselves to some more general remarks that we illustrate using ALEPH. Results will be given for each of the collaborations and then combined to give a LEP result.

4.1 Event triggers

Highly efficient triggering on all four event classes turned out to be relatively easy at LEP because of low background rates. All detectors use multiple ORed triggers. The trigger redundancy (25 in the case of ALEPH) not only serves to obtain high efficiency, but, and perhaps more important, it makes it possible to *measure* the efficiency. Triggering efficiencies of very nearly 100% for each of the four event types, and with uncertainties of less than 0.1%, are obtained.

4.2 Event selection

The four channels have very distinct characteristics, as can be seen from Fig 17. The dominant channel is the $q\bar{q}$ channel, with 88% of the observed events. These events have typically many charged tracks, on the average 20, and large energy deposits in both calorimeters, with total energy near the center-of-mass energy. The e^+e^- events are characterized by two back-to-back tracks, each with the momentum equal to the beam energy, with the full energy in the electromagnetic calorimeter. The $\mu^+\mu^-$ events have two back-to-back tracks which penetrate the hadron calorimeter, with very little calorimetric

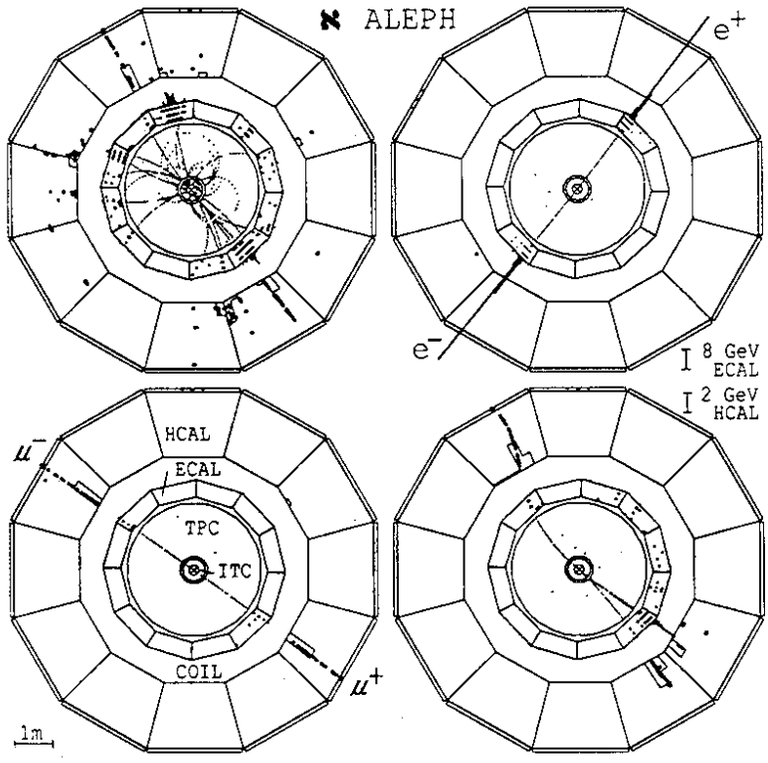

Fig. 17 Typical events for each of the four channels. (From ALEPH.)

energy. The $\tau's$, depending on their decay, each have one or three tracks, typically with substantial missing energy, and are also back-to-back. These characteristics can be modified by initial- or final-state radiation, and by the interaction of the outgoing particles in the beam pipe and detector, but it is, in general, possible to separate the channels with purities exceeding 99%, with little loss in efficiency. The dominant background, the e^+e^- inelastic scattering (the two-photon channel) with the production of additional particles, can be dealt with on the basis of the typically small energy and the forward–backward energy imbalance of these events.

The selection efficiencies and purities are determined using Monte Carlo simulations of the different event channels and backgrounds. The acceptances are close to unity, with a small uncertainty for hadronic ($q\bar{q}$) events (99.1 $\pm$ 0.2% in ALEPH) and somewhat larger inefficiencies and uncertainties for leptons, especially $\tau's$ (98.4 $\pm$ 0.3% for the combined ALEPH lepton sample).

Event generators for all channels exist with a high precision and ability to reproduce the observed events[13], and all four detectors have been simulated in full detail. As an example, Fig. 18 reproduces data and simulations for the thrust axis of hadronic events observed in ALEPH.

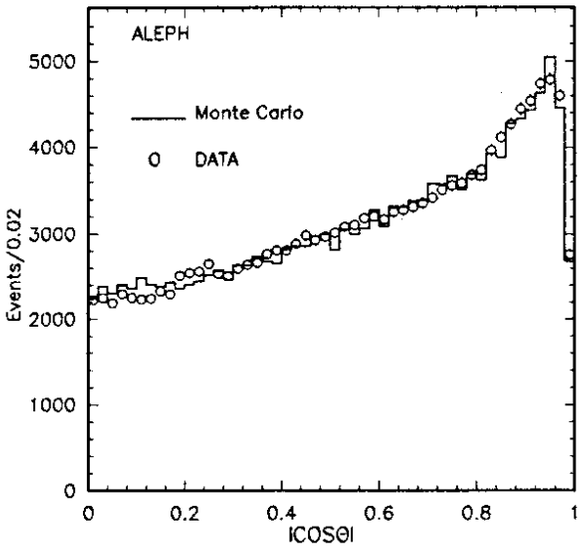

Fig. 18 Check on the validity of the acceptance calculation for hadronic events. Comparison of simulation and data for the thrust axis distribution. (From ALEPH.)

4.3 Luminosity measurement

The luminosity is measured, as has always been the case at e^+e^- colliders, with the help of Bhabha scattering, at angles small enough so that the cross-section is dominated by the t channel, and the contribution of Z-exchange interference is a small correction. The luminosity detectors of the four collaborations work in the angular region between 40 and 120 mrad. It is interesting that the theoretical uncertainties in the Bhabha cross-section[14] contribute non-negligibly to the error as the experimental precision improves. The experimental challenge is that of defining the geometrical acceptance with high accuracy. In the case of ALEPH, the luminosity detector is a lead–proportional wire sandwich calorimeter covering the small-angle region on each side. It is read out with high angular resolution in

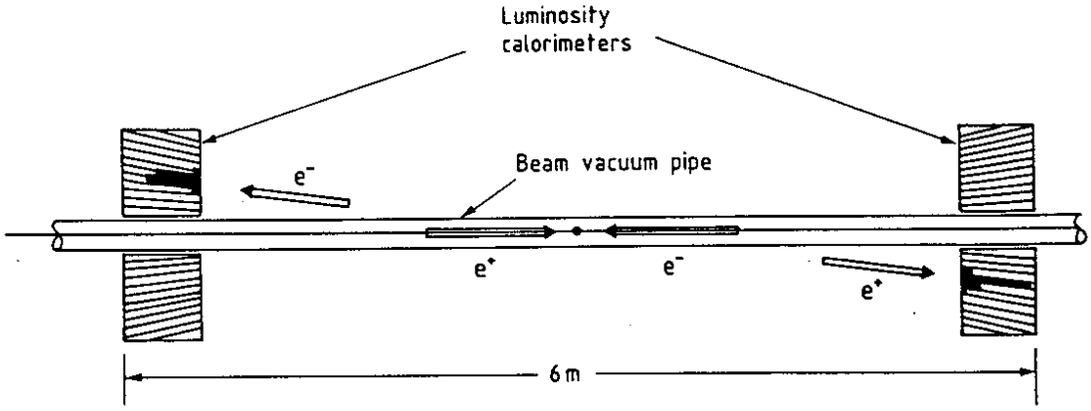

Fig. 19 Disposition of the luminosity calorimeter in ALEPH.

754 projective towers (see Fig. 19). One side, which alternates from event to event, is geometrically more restrictive and defines the fiducial acceptance. The angular uncertainty in the fiducial boundary, event by event, is about 0.08 mrad, and the total systematic uncertainties in the luminosity are 0.4%. The L3 experiment also uses a segmented calorimeter, which however is not projective and gives an experimental uncertainty of 0.7%. Figure 20 shows the precision with which the angular acceptance is understood in this detector. The DELPHI experiment uses masked calorimeters and quotes an error of 0.8%. The OPAL experiment uses proportional tubes inserted into a segmented calorimeter after the first four radiation lengths, to define the geometrical acceptance for the absolute cross-section measurement with a precision of 0.7%.

The theoretical uncertainty in the most recent Bhabha calculations[15] is believed to be $\sim 0.5\%$.

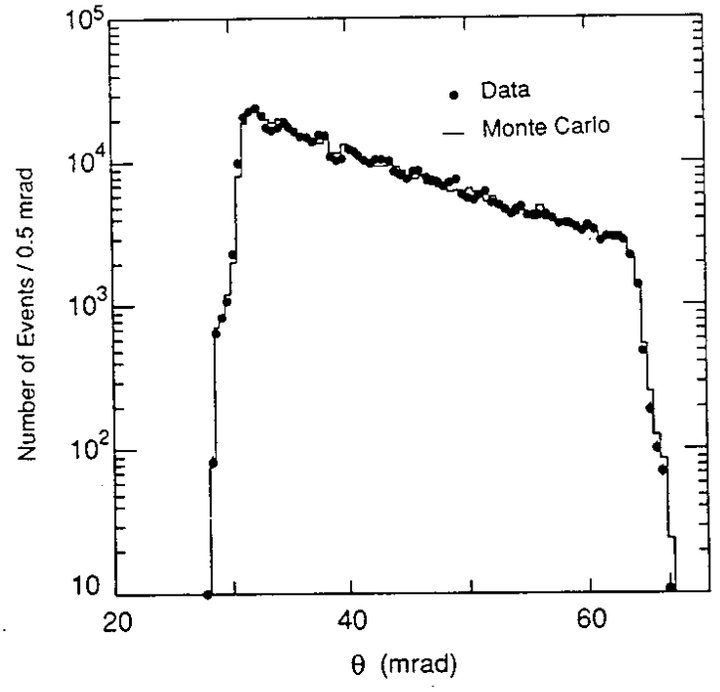

Fig. 20 Check on the validity of the acceptance calculation for luminosity events. Comparison of simulation and data for the polar angle distribution. (From L3.)

4.4 LEP beam energy

One of the important results of these first measurements at LEP is the measurement of the Z mass: m_Z is the energy of the center-of-mass collision, twice the beam energy at the pole of the Z resonance. The precise knowledge of this energy is therefore essential to this measurement. The calibration of the LEP beam energy is at present based on the measurement of the frequency difference between protons and positrons circulating in the same LEP orbit at $\sim$ 20 GeV. The relative increase in beam energy from 20 to 45 GeV is established using flux loops on each of the LEP magnets. The present uncertainty is 20 MeV in the c.m. energy (0.22 parts per thousand)[16]. In the future it is expected that even higher precision will be achieved, using the precession frequency of transversely polarized beam electrons.

4.5 Results on the Z line shape and the number of fermion families

The most comprehensive results which can be included in this review are those presented by the four collaborations at a recent conference in Aspen[17]. They are based on all data obtained in 1989 and 1990. They are preliminary, but substantial changes are not expected before publication. They are based on the event numbers and acceptances of Table 1. Major parts of these results have been published previously[18].

Table 1

Numbers of selected events ($N_{ev.}$), angular acceptances, as well as acceptance efficiencies for the four experiments and the four dominant Z decay channels

Channel	Parameters	ALEPH	DELPHI	L3	OPAL
$q\bar{q}$	$N_{ev.}$	175,000	120,000	115,000	166,000
	Ang. accept.	4π	4π	4π	4π
	Efficiency (%)	99.1±0.2	96.9±0.5	99.0±0.4	98.4±0.6
e^+e^-	$N_{ev.}$	6942	2615	4175	5415
	Ang. accept.	$\cos\theta\ ^{-\ 0.9}_{+\ 0.7}$	$\lvert\cos\theta\rvert < 0.7$	$\lvert\cos\theta\rvert < 0.7$	$\lvert\cos\theta\rvert < 0.7$
	Efficiency (%)	98.8±0.4	97.3±0.7	99.2±0.6	99.3±0.7
$\mu^+\mu^-$	$N_{ev.}$	6691	2489	3245	7240
	Ang. accept.	$\lvert\cos\theta\rvert < 0.9$	$\lvert\cos\theta\rvert < 0.93$	$\lvert\cos\theta\rvert < 0.8$	$\lvert\cos\theta\rvert < 0.95$
	Efficiency (%)	99.6±0.6	91.5±0.8	78.3±0.6	91.6±0.5
$\tau^+\tau^-$	$N_{ev.}$	6260	2039	2540	5559
	Ang. accept.	$\lvert\cos\theta\rvert < 0.9$	$\lvert\cos\theta\rvert < 0.73$	$\lvert\cos\theta\rvert < 0.7$	$\lvert\cos\theta\rvert < 0.9$
	Efficiency (%)	85.4±0.7	87±1.4	75.4±1.6	86.1± 1.1
$\ell^+\ell^-$	$N_{ev.}$	24757	9676		
	Ang. accept.	$\lvert\cos\theta\rvert < 0.9$	$\lvert\cos\theta\rvert < 0.69$		
	Efficiency (%)	98.4±0.3	90.1±0.6		

The basic results on the line shape are the cross-sections for the four channels: $q\bar{q}$, e^+e^-, $\mu^+\mu^-$, and $\tau^+\tau^-$ as a function of the center-of-mass energy. Figure 21 shows the OPAL result for the hadronic channel, and Fig. 22 the ALEPH results for the leptonic channels. From these, the parameters m_Z, Γ_Z, and σ^{peak} can be found by fitting the model-independent resonance expression (1) [19]. It is common practice now to obtain m_Z and Γ_Z

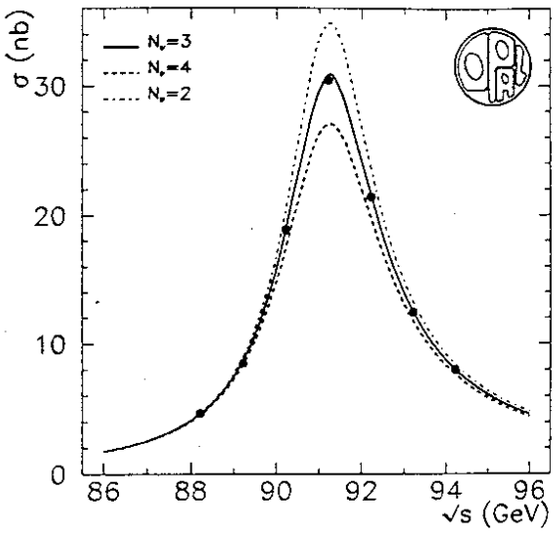

Fig. 21 Cross-section for the reaction $e^+e^- \rightarrow q\bar{q} \rightarrow$ hadrons as a function of the center-of-mass energy. The electroweak expectations for 2, 3, and 4 families are shown, with one fitted free parameter, the Z mass. (From OPAL.)

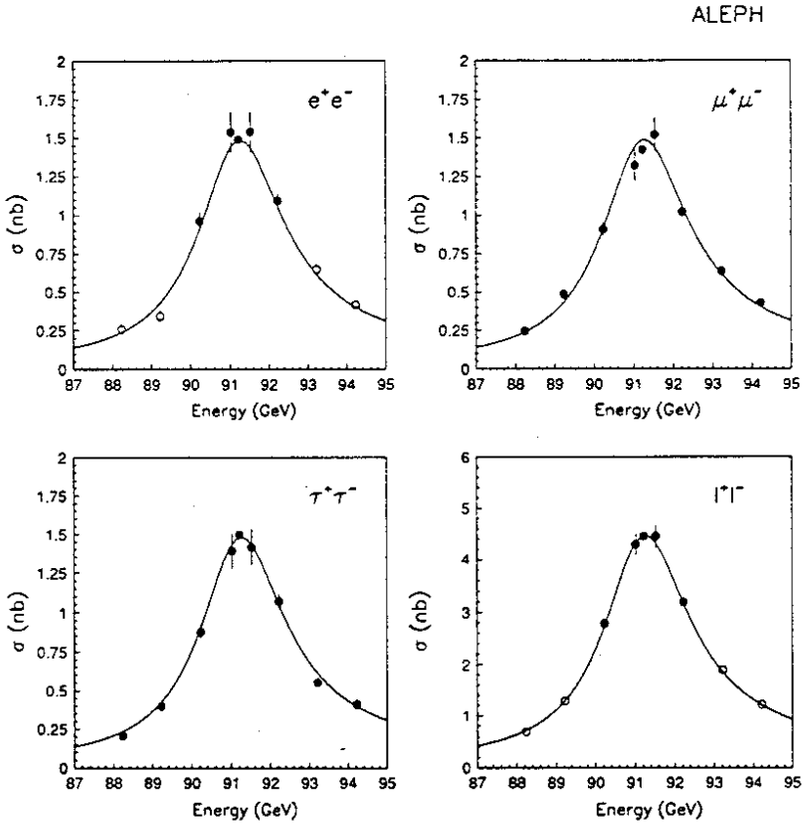

Fig. 22 Cross-section as a function of the center-of-mass energy for each of the three lepton channels, as well as the combined channel. The t-channel contribution for the electron channel has been subtracted. (From ALEPH.)

from a combined fit to all channels. The partial widths are derived from Γ_Z and the peak cross-sections as follows:

$$\begin{aligned} \Gamma_h &= m_Z \Gamma_Z \sqrt{R\sigma_h^{peak}/12\pi}, \\ \Gamma_{e,\ell} &= m_Z \Gamma_Z \sqrt{\sigma_{e,\ell}^{peak}/12\pi}, \\ \Gamma_{\mu,\tau} &= m_Z \Gamma_Z \sigma_{\mu,\tau}^{peak} / \sqrt{12\pi\sigma_e^{peak}} \end{aligned}$$

and

$$\Gamma_{\rm inv} = \Gamma_{\rm Z} - \Gamma_{\rm h} - 3\Gamma_\ell = \Gamma_{\rm Z}\left(1 - \sqrt{R\sigma_{\rm h}^{\rm peak} m_{\rm Z}^2/12\pi} - 3\sqrt{\sigma_{\rm h}^{\rm peak} m_{\rm Z}^2/12\pi R}\right) ,$$

where $R = \sigma_{\rm h}^{\rm peak}/\sigma_\ell^{\rm peak}$. The subscript ℓ denotes the average of the three leptonic channels, assuming universality.

The results of the four collaborations are given in Table 2. There are no significant disagreements. The errors quoted include both statistical and systematic errors. In the combined results, the common theoretical uncertainty in the luminosity Bhabha cross-section, taken to be 0.5%, has been included. Other possible sources of common systematic errors include the t-channel treatment in wide-angle Bhabha scattering and a point-to-point error in the LEP energy calibration affecting the width measurement. We believe that, at present, these common errors can still be neglected.

Table 2
Results of the four LEP experiments on the Z line shape and partial decay widths

Result	ALEPH	DELPHI	L3	OPAL	Combined LEP result
$m_{\rm Z}$, GeV	91.182 ±0.009	91.175 ±0.010	91.180 ±0.010	91.160 ±0.009	91.174 ±0.005 ± 0.020 LEP
$\Gamma_{\rm Z}$, MeV	2488 ±17	2454 ±20	2500 ±17	2497 ±17	2487 ±9
$\sigma_{\rm h}^{\rm peak}$, nb	41.76 ±0.39	41.98 ±0.63	40.92 ±0.47	41.23 ±0.47	41.46 ± 0.29
$\Gamma_{\rm h}$, MeV	1756 ±15	1718 ±22	1739 ±19	1747 ±19	1744 ±10
$\Gamma_{\rm e}$, MeV	84.2 ±0.9	81.6 ±1.3	83.0 ±1.0	83.5 ±1.0	83.3 ± 0.5
Γ_μ, MeV	80.9 ±1.4	88.4 ±2.4	84.3 ±2.0	83.5 ±1.5	83.3 ±0.9
Γ_τ, MeV	82.9 ±1.6	84.9 ±2.7	83.3 ±2.6	83.1 ±1.9	83.3 ±1.0
Γ_ℓ, MeV	83.3 ±0.7	83.4 ±1.0	83.3 ±0.8	83.4 ±0.7	83.3 ±0.4
$R = \Gamma_{\rm h}/\Gamma_\ell$	21.07 ±0.19	20.61 ±0.33	20.88 ±0.28	20.94 ±0.24	20.94 ±0.12
$\Gamma_{\rm inv.}$, MeV	481 ±14	486 ±21	511 ±18	499 ±17	493 ±9.5
N_ν, MeV	2.90 ±0.08	2.93 ±0.13	3.08 ±0.10	2.99 ±0.10	2.96 ±0.06

The three lepton partial widths are equal at their level of precision of $\sim$ 1%, in agreement with the universality of the weak interaction.

One of the important consequences of these results concerns the number of fermion families. In the Standard Model, each light neutrino family contributes 166.5 ± 0.5 MeV

(assuming the top mass to be $90 < m_t < 160$ GeV and the Higgs mass to be $50 < m_H < 1000$ GeV) to the 'invisible width' $\Gamma_{inv} = \Gamma_Z - \Gamma_h - 3\Gamma_\ell$. There is no evidence for fermions other than those of the three known families, but fermions with masses exceeding the reach of present-day accelerators can be postulated. However, for the known families, the neutrino masses are, if not zero, much less than the masses of their charged counterparts, at least by a factor of a hundred. In the absence of a theory of the masses, it is at least very plausible to assume that the neutrinos of higher families would still have masses well below one-half the Z mass. They would then contribute to the invisible width. So would any other non-detected neutral channels, such as other weakly interacting particles emitted in the decay of the Z.

From the experimental result $\Gamma_{inv} = 493 \pm 9.5$ MeV, and with the above theoretical value of the neutrino partial width, Γ_ν,

$$N_\nu = 2.96 \pm 0.06 \ .$$

The result leaves no room for a fourth fermion family, and little room for any other new neutral weakly interacting particle. If one wants to imagine a fourth neutrino family with mass only slightly less than $m_Z/2$, the error on the result for Γ_{inv} corresponds to a lower mass limit of 45.5 GeV for a Dirac type of neutrino, and of 42.3 GeV for a Majorana type, at 95% confidence level.

The fact that the result is 3 and not 2 is striking confirmation of the separate identity of the τ neutrino, although strong evidence for this already exists in the experimental results on τ decay, which are in good agreement with the electroweak theory. Finally, the fact that N_ν is, with good precision, compatible with an integer is an interesting confirmation of the Standard Model.

4.6 Lepton forward–backward and τ polarization asymmetries

In principle, the forward–backward asymmetries can be measured for all eight types of charged fermions, and so the v^2/a^2 ratio measured independently for every one. Measurements of each of the three lepton channels have been reported by all four collaborations[18]; the statistical significance is however still limited. The results are in agreement with universality. Here we content ourselves with reporting only the combined lepton results. The quark flavors are not, in general, separable; however, with limited efficiency and purity, the b channel can be separated; the b-quark asymmetry has been reported by the ALEPH and L3 collaborations[20]. A global quark forward–backward asymmetry, based on the overall charges assigned to the jets, has been reported by ALEPH[21].

In the determination of polarization asymmetries, only the effects of initial beam polarization and the τ polarization are measurable. The former, which offers the possibility of very precise measurements of v/a, waits for the development of longitudinaly polarized beams. However, the τ polarization can be measured using the energy distributions of the decay products in various decay channels. A first result has been reported by ALEPH[22].

A typical result on the lepton angular distribution is shown in Fig. 23. It illustrates also a particular problem of the e^+e^- channel: the important contribution of the t-channel photon exchange at small angles. This is a QED process, calculated[23] and subtracted. Figure 24 shows the dependence of the asymmetry on the center-of-mass energy, together with a two-parameter (v, a) electroweak fit. The interesting point is the very small asymmetry on the resonance peak. The much larger asymmetries, away from the peak, are due

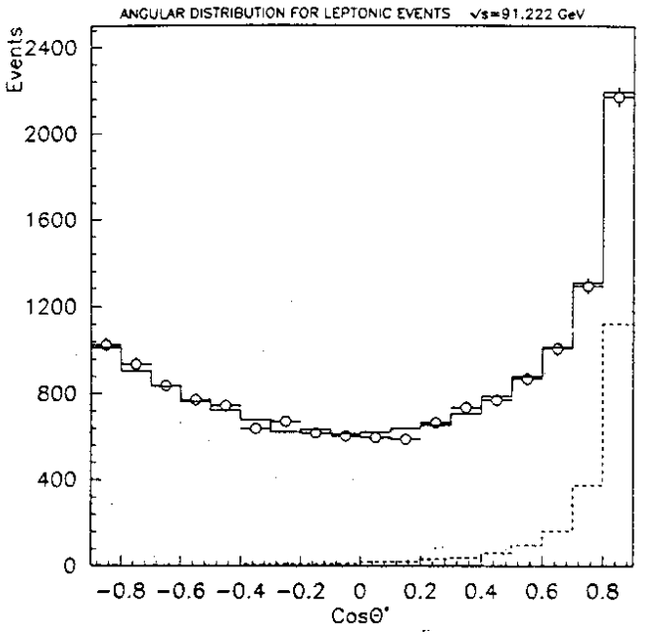

Fig. 23 Angular distribution of the combined leptonic channels on the Z resonance peak. The calculated t channel $e^+e^- \to e^+e^-$ contribution is also shown. (From ALEPH.)

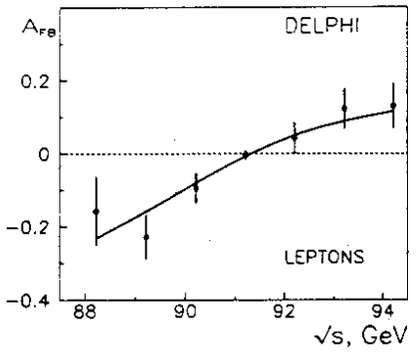

Fig. 24 The leptonic forward–backward asymmetry, $A_{\rm FB}^{\ell}$, as a function of the center-of-mass energy. Only thevery small asymmetry at the Z peak is dominated by v_ℓ^2/a_ℓ^2. The rest is dominated by Q_ℓ^2/a_ℓ^2. (From DELPHI.)

to the interference of the axial weak current with the electromagnetic (vector) current. As already noted in Section 3.3.1, the asymmetry on the peak measures the ratio of vector to axial-vector current strengths: $A_{\rm FB}^{\ell} \simeq 3v_\ell^2/a_\ell^2$.

This result can be combined with the measurement of the partial leptonic width to obtain both leptonic vector and axial-vector couplings independently of the details of the electroweak theory. For this purpose, it is customary to introduce the coupling constants $g_{\rm V,f}$ and $g_{\rm A,f}$, incorporating the Fermi constant, by rewriting expression (7), using Eq. (10):

$$\Gamma_{\rm f} = \frac{\sqrt{2} G_{\rm f} m_{\rm Z}^3 N_{\rm c}^{\rm f}}{12\pi} (g_{\rm V,f}^2 + g_{\rm A,f}^2) \ .$$

In the electroweak theory $g_{\rm V}$ and $g_{\rm A}$ are related to the mixing angle:

$$g_{\rm V,f} = \sqrt{\rho}(I_3^{\rm f} - 2Q_{\rm f}\,\overline{\sin^2\theta_{\rm w}}) = \sqrt{\rho}\ v_{\rm f} \cdot 2\,\overline{\sin\theta_{\rm w}\cos\theta_{\rm w}}$$

and

$$g_{\rm A,f} = \sqrt{\rho} I_3^{\rm f} = \sqrt{\rho}\ a_{\rm f} \cdot 2\,\overline{\sin\theta_{\rm w}\cos\theta_{\rm w}} \ .$$

Of course, $g_{\rm V,f}/g_{\rm A,f} = v_{\rm f}/a_{\rm f}$. In the electroweak theory $v_\ell/a_\ell = 1 - 4\,\overline{\sin^2\theta_{\rm w}}$, so that the leptonic forward–backward asymmetry (for that matter the other asymmetries as well) provides a measure of the 'effective' mixing angle without complication of top or Higgs corrections.

Table 3

Result of the combined lepton sample for the asymmetry A_{FB}^{ℓ} on the Z peak, the ratio of vector to axial vector coupling strengths, and $g_{V,\ell}^2$ and $g_{A,\ell}^2$

	ALEPH	DELPHI	L3	OPAL	Combined LEP result
A_{FB}^{ℓ}	0.024 $\pm$0.008	0.008 $\pm$0.013	0.024 $\pm$0.014	0.007 $\pm$0.008	0.016 $\pm$ 0.005
v_ℓ^2/a_ℓ^2	0.0082 $\pm$0.0026	0.0028 $\pm$0.0044	0.0080 $\pm$0.0048	0.0023 $\pm$0.0028	0.0054 $\pm$ 0.0016
$g_{V,\ell}^2$	0.0020 $\pm$0.0007	0.0007 $\pm$0.0014	0.0020 $\pm$0.0012	0.0006 $\pm$0.0007	0.0014 $\pm$ 0.0004
$g_{A,\ell}^2$	0.2484 $\pm$0.0022	0.2510 $\pm$0.0028	0.2490 $\pm$0.0030	0.2509 $\pm$0.0022	0.2498 $\pm$ 0.0012
$\overline{\sin^2\theta_w}$					$0.2317\ ^{+\ 0.0030}_{-\ 0.0026}$

The results for the lepton asymmetry, v_ℓ/a_ℓ, and $g_{V,\ell}$ and $g_{A,\ell}$ are given in Table 3 for the combined lepton sample.

For the measurement of the b-quark forward-backward asymmetry, the b channel is selected using electronic and muonic b decay, which together account for 20% of b decay. The main backgrounds are due to the leptonic decay of charm quarks and to hadrons misidentified as leptons. The requirement of high lepton momentum as well as transverse momentum increases the purity of the sample at the expense of efficiency (see Fig. 25). Typical values are 80% and 10% respectively.

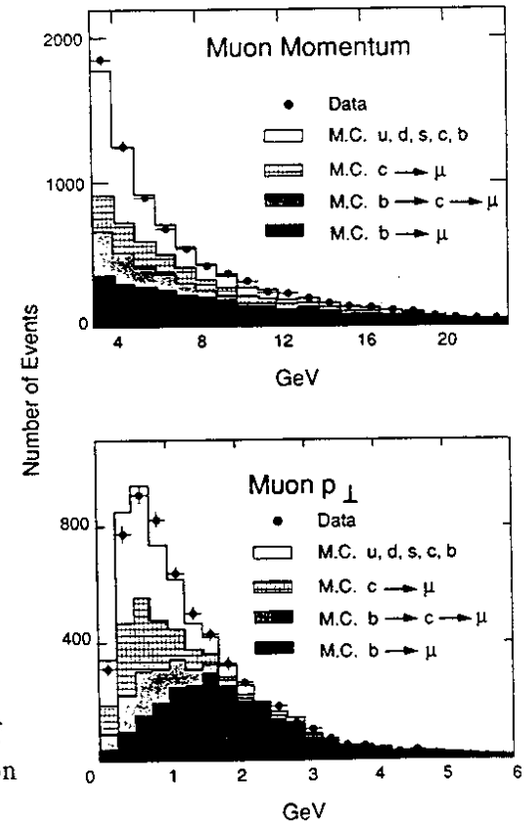

Fig. 25 Purity of the b-quark channel as a function of the momentum and transverse momentum of the lepton is used to tag the channel. (From L3.)

As seen in Section 3.3.1, on the Z pole:

$$A_{FB}^{b} = \frac{3[(v_\ell/a_\ell)(v_b/a_b)]}{[1+(v_\ell/a_\ell)^2][1+(v_b/a_b)^2]} .$$

Since $v_b/a_b = 1 - \frac{4}{3}\overline{\sin^2\theta_w} \simeq 0.69$ is about ten times larger than v_ℓ/a_ℓ, the b asymmetry would be potentially more sensitive to $\sin^2\theta_w$ than the leptonic asymmetry. But this is more than compensated, at present, by the combined effect of selection inefficiency and impurity of the b sample.

In addition, there is the effect of $b\bar{b}$ mixing. In first approximation the b ($\bar{b}$) is identified by a positive (negative) lepton, and this is always valid for the charged B mesons. However, the neutral B^0 ($\bar{B}^0$) meson can transform into its charge conjugate before decay, and so falsify the signature. The $B\bar{B}$ mixing parameter, $\chi \equiv$ number of charge conjugate decays/total number of b decays, is measured using events with two leptons, one associated with each jet. After background corrections, χ is obtained from the number of like-sign double-lepton events, normalized to the total number of double-lepton events.

The observed asymmetry must be corrected for this mixing. The experimental results for the mixing[24] are included in Table 4, which gives the b-asymmetry results for the ALEPH and L3 collaborations[20].

Table 4
The observed $b\bar{b}$ forward-backward asymmetries A_{FB}^{b}, the observed mixing parameter χ, the corrected forward-backward asymmetry $A_{FB,corr.}^{b}$, as well as the corresponding weak mixing angle, for the ALEPH and L3 collaborations, as well as the combined result

	ALEPH	L3	Combined result
A_{FB}^{b}	0.104 ± 0.025	0.084 ± 0.025	0.094 ± 0.018
χ	$0.132 \pm^{0.027}_{0.026}$	$0.178 \pm^{0.049}_{0.040}$	$0.144 \pm^{0.25}_{0.22}$
$A_{FB,corr.}^{b}$	0.141 ± 0.044	$0.130 \pm^{0.044}_{0.042}$	0.135 ± 0.031
$\overline{\sin^2\theta_w}$	0.225 ± 0.008	0.226 ± 0.008	0.226 ± 0.006

The τ polarization on the Z peak is a measure of v_τ/a_τ [see Eq. (15)]:

$$\langle P_\tau \rangle = A_{pol}^{\tau} = \frac{-2v_\tau/a_\tau}{1+(v_\tau/a_\tau)^2} .$$

It can be inferred from the energies of the decay products, which in turn reflect the angle of decay in the τ rest system.

The sensitivity to the polarization varies substantially from one decay channel to another. The hadronic decay channels $\tau \to \nu_\tau + \pi$ and $\tau \to \nu_\tau + \rho$ are more useful here than

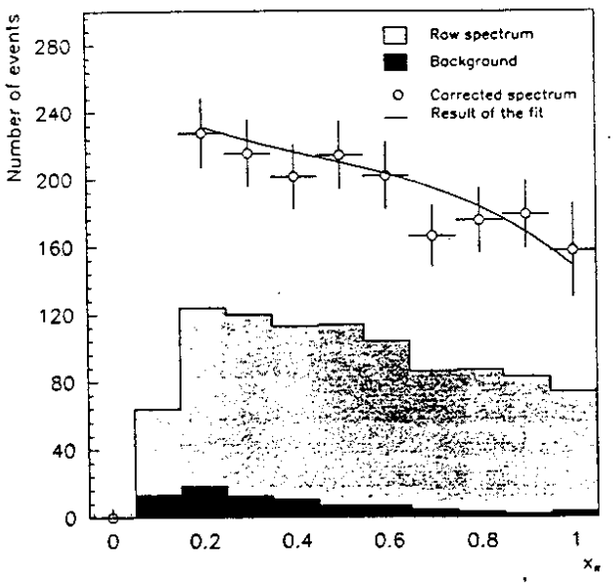

Fig. 26 Energy spectrum of pions in the channel $e^+e^- \to \tau^+\tau^-$, $\tau \to \pi + \nu_\tau$, used to measure the τ polarization. A flat spectrum corresponds to no polarization. Helicity $+1$ (-1) corresponds to a linear spectrum with zero at the maximum (minimum) pion energy. (From ALEPH.)

the leptonic channels. The only result at present is that of ALEPH[22]. Figure 26 shows the energy spectrum of the pion in the channel $\tau \to \nu_\tau + \pi$. Positive helicity corresponds to a linear distribution that is zero at $E_\pi = E_{\max}$, negative to a distribution going to zero at $E_\pi = 0$. The slope of the observed distribution gives the τ polarization. In addition the $\rho\nu, a_1\nu$, and leptonic decay channels have been studied, with the result

$$A^\tau_{\rm pol} = \langle P_\tau \rangle = -0.157 \pm 0.055 \text{ (Ref. 22)}.$$

This corresponds to $\overline{\sin^2\theta_{\rm w}} = 0.231 \pm 0.007$.

Some measure of the forward–backward asymmetry of the sum of all quarks can be obtained from the asymmetry in the momentum-weighted charges of the jets. Such a study has been performed by ALEPH[21]. The hadronic events are divided into two jets by a plane perpendicular to the thrust axis. The 'charge' of each jet is determined by summing the charges of individual tracks multiplied by a power of their momentum. By simulation it is found that the power 1 maximizes the sensitivity, and it is thus chosen. Still on the basis of simulation, the charge asymmetries expected for each of the five quark flavors are determined. These differ substantially from flavor to flavor, and are negative for up-type, and positive for down-type quarks. Only a small net charge asymmetry remains, but the statistical error is correspondingly small, because of the large number of hadronic events:

$$A_{{\rm FB},Q} \equiv \langle Q_{\rm forward} - Q_{\rm backward} \rangle = 0.0084 \pm 0.0016 \ .$$

This net asymmetry is the flavor average of the forward–backward asymmetries multiplied by the product of the production fraction $p_{\rm f}(\Sigma p_{\rm f} = 1)$, times the average jet charge expected for a given quark, $q^{\rm jet}_{\rm f}$:

$$A_{{\rm FB},Q} = 3 \sum_{\rm f} \frac{v_{\rm e}}{a_{\rm e}} \ \frac{v_{\rm f}/a_{\rm f}}{(1 - v^2_{\rm f}/a^2_{\rm f})} p_{\rm f} q^{\rm jet}_{\rm f} \ .$$

An uncertainty of 18% is assigned to the determination of the $q^{\rm jet}_{\rm f}$ on the basis of quark hadronization programs. The result, in terms of $\overline{\sin^2\theta_{\rm w}}$, is

$$\overline{\sin^2\theta_w} = 0.2300 \pm 0.0053 \ .$$

combining all asymmetry measurements available at present, this value is: $\overline{\sin^2\theta_w} = 0.2306 \pm 0.0022$.

5 COMPARISON OF THE RESULTS ON THE Z RESONANCE WITH THE STANDARD MODEL

The electroweak theory is defined by two coupling constants, the mixing angle, the masses of the fermions, and the mass of the Higgs. The coupling constants can be taken to be the fine structure constant α and the Fermi constant G_F. Instead of the mixing angle, it is convenient to use the Z mass m_Z. One of the important results of these experiments is therefore the more precise value of $m_Z = 91.174 \pm 0.021$ GeV as compared with the most precise previous results:

UA2	m_Z	$= 91.49 \pm 0.99$ GeV	(Ref. 25)
CDF	m_Z	$= 90.9 \pm 0.4$ GeV	(Ref. 26)
SLAC	m_Z	$= 91.14 \pm 0.12$ GeV	(Ref. 27)

Fermion masses and the Higgs mass enter through the radiative corrections to the partial widths, cross-sections, and asymmetries. The precise measurements of these quantities at the Z peak therefore permit some insight into the as-yet-unknown top and Higgs masses. As pointed out in Section 3.2, the dominant but not exclusive correction involving the top and Higgs masses is through $\Delta\rho$, where they occur approximately in the combination:

$$\Delta\rho \simeq 0.0026 m_t^2/m_Z^2 - 0.0015 \ln (m_H/m_W) \ .$$

In order to separate the effects of m_t and m_H it is therefore necessary, at least until the top is seen and its mass measured, to use the fact that some parameters, such as Γ_b, have m_t dependences not contained in ρ. This separation is not possible at present levels of precision at LEP. However, for the mass interval imagined as possible for the Higgs, $50 < m_H < 1000$ GeV [a lower bound of ~ 50 GeV has been established by the LEP experiments[28]], the top-mass effect dominates. The main measured quantities relevant to a determination of this radiative correction and the top mass are $m_Z, m_W, \Gamma_Z, \Gamma_\ell$, and $\overline{\sin^2\theta_w}$ as measured in the asymmetries. Four of these are measured at LEP, the fifth, m_W, is obtained from the ratio m_W/m_Z, measured in the $p\bar{p}$ collider experiments[29] and in the ratio of neutral- to charged-current deep-inelastic neutrino scattering[30]. The combined result for m_W, given the LEP result for m_Z, is $m_W = 80.05 \pm 0.22$ GeV.

For a particular Higgs mass, each of these quantities can be seen as a relationship between the top mass and the effective mixing angle, as shown in Fig. 27 for $m_H = 200$ GeV. If the lower limit on the top mass, obtained in the direct search by the CDF collaboration at Fermilab, $m_t > 89$ GeV, at the 90% confidence level[31], is included, Fig. 27 shows everything known at present about the top mass as well as all the accurate information on the mixing angle. It also shows much of the relevant information about the consistency of the LEP results with the Standard Model, which is just the fact that the

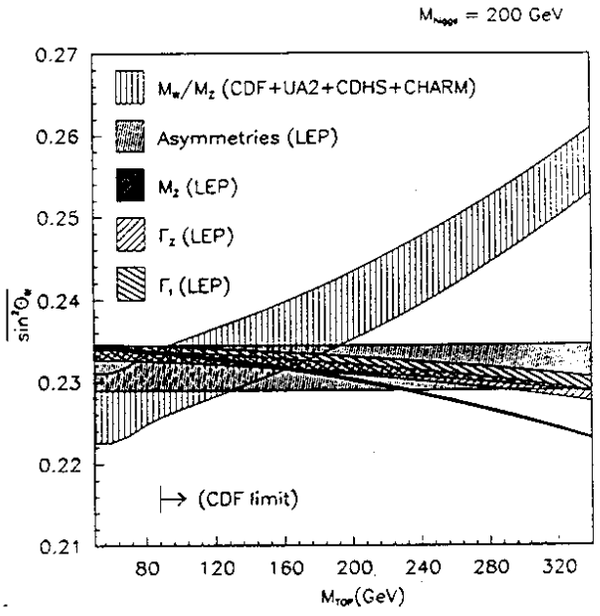

Fig. 27 Correlation between $\overline{\sin^2\theta_w}$ and m_t for $m_Z, m_W, \Gamma_Z, \Gamma_\ell$, and the asymmetries, for a Higgs mass $m_H = 200$ GeV. This plot permits a visualization of the information furnished by these measurements towards our knowledge of $\overline{\sin^2\theta_w}$ and m_t through the radiative corrections, as well as the compatibility of these measurements in the frame of the electroweak theory.

five experimental bands share a common area or, in other words, that best fits of $\overline{\sin^2\theta_w}$ and m_t can be found with the correct χ^2. These are

$$\begin{aligned} \overline{\sin^2\theta_w} &= 0.2327 \pm 0.0008 \pm 0.0003(m_H) \\ m_t &= 126 \pm 30 \pm 18(m_H)\ \text{GeV} \\ \chi^2 &= 1.4/4\ \text{degrees of freedom.} \end{aligned}$$

The precision of the new value of $\sin^2\theta_w$ is dominantly due to the precision in m_Z; Γ_ℓ, Γ_Z, and m_W contribute comparably to the limitation on the top mass.

In Table 5 the Standard Model expectations are given for the various measured quantities, as well as the value of $\overline{\sin^2\theta_w}$ which follows from them. The Standard Model

Table 5

Combined LEP results and Standard Model predictions for $m_Z, \sigma_h^{peak}, \Gamma_Z$, $\Gamma_h, \Gamma_\ell, R, N_\nu$, and asymmetries. In the prediction the measured values of m_Z are used, as well as $\alpha_s = 0.120 \pm 0.008, m_t = 125 \pm 35$ GeV, and $50 < m_H < 1000$ GeV. The column in $\overline{\sin^2\theta_w}$ lists the value which follows from the particular experiment.

	Experiment	Standard Model	$\overline{\sin^2\theta_w}$
m_Z, GeV	91.174 ± 0.021		0.2327 ± 0.0012
Γ_Z, MeV	2487 ± 9	2486 ± 10	0.2327 ± 0.0010
σ_h^{peak}, nb	41.46 ± 29	41.42 ± 0.05	0.2328 ± 0.0026
Γ_h, MeV	1744 ± 10	1737 ± 8	0.2320 ± 0.0012
Γ_ℓ, MeV	83.5 ± 0.4	83.6 ± 0.3	0.2331 ± 0.0014
$R = \Gamma_h/\Gamma_\ell$	20.94 ± 0.12	20.80 ± 0.06	0.225 ± 0.010
Γ_{inv}	493 ± 9.5	499 ± 2	0.2356 ± 0.0037
N_ν	2.96 ± 0.06	Integer	
$(v/a)_\ell^2$ from A_{FB}^ℓ	0.0054 ± 0.0016	0.0048 ± 0.0007	$0.2317 \pm^{0.0030}_{0.0026}$
$(v/a)_\tau$ from $A_{\tau,pol}$	0.079 ± 0.028	0.069 ± 0.005	0.231 ± 0.007
A_{FB}^b	0.135 ± 0.031	0.097 ± 0.007	0.226 ± 0.006
$A_{FB,Q}$	0.0084 ± 0.0016		0.2300 ± 0.0053

expectations assume $90 < m_t < 160$ GeV, $50 < m_H < 1000$ GeV, and, where relevant, $\alpha_s = 0.120 \pm 0.008$. The agreement with the Standard Model can be judged both in comparing the experimental and theoretical values and in comparing the results for $\sin^2\theta_w$ with one another and with the value of 0.2327 ± 0.0012 that follows from m_Z. The results for Γ_Z, Γ_ℓ, and the asymmetries are largely independent of each other, and each checks the model at a level of $\Delta \sin^2\theta_w \sim 0.001$–$0.002$.

The predictions for σ_h^{peak} and R are approximately independent of the top and Higgs radiative corrections, since they are ratios of widths, and in the ratio these corrections nearly cancel. They reflect however the uncertainty in α_s through the QCD radiative correction of Γ_h. This introduces the main theoretical uncertainty, $\sim 0.3\%$ in R and $\sim 0.1\%$ in σ_h^{peak}. The two measurements confirm the structure of the theory at the 0.5% level.

The strong coupling constant at the Z mass, $\alpha_s(m_Z^2)$, can be deduced from the measured values of Γ_Z and R, because of the QCD correction $(1 + \alpha_s/\pi + 1.4\ \alpha_s^2/\pi^2)$ of the hadronic partial widths. With $m_t = 125 \pm 35$ GeV and $50 < m_H < 1000$ GeV,

$$\alpha_s = 0.119 \pm 0.028 \text{ from } \Gamma_Z \ ,$$
$$\alpha_s = 0.146 \pm 0.022 \text{ from } R \ ,$$

and, combined,

$$\alpha_s = 0.136 \pm 0.017 \text{ (statistical error only)} \ .$$

This result is not statistically as precise as those derived from the shape parameters of hadronic events, but is useful because it has different systematic uncertainties.

6 SUMMARY AND FUTURE

The results of the cross-section measurements on and near the Z peak during this first year of LEP operation, based on the analysis of $\sim 700,000$ Z decay events by the four experimental collaborations, have shown that there are just three neutrino families with mass less than $m_Z/2$, and therefore very probably just three fermion families; the mass of the Z has been measured with a precision of 1 part in 4000, and the predictions of the Standard Model have been verified at a level of approximately one-half of a per cent for the total Z widths, for partial Z decay widths, and for asymmetries in the angular distributions. No evidence for inadequacy of the Standard Model, which might indicate new directions in physics, has been found. A rough value for the mass of the top is obtained through the contributions of the top to radiative corrections. Other results of this first operation, such as new particle searches, QCD studies, and heavy-quark studies, are not reported here.

A program to increase the LEP energy above the W^+W^- production threshold should be completed in 1994; this will make it possible to study other electroweak processes, such as the coupling of the Z to a W^+W^- pair. Given sufficient luminosity and time, it will also permit a measurement of the W mass with an error of about 75 MeV, three times better than the present value.

In the meantime, before the higher energy is available, it is expected that the integrated luminosity at and near the Z peak will be increased by a factor of 10 or more, with consequent improvement in sensitivity to deviations from the Standard Model. It is also hoped that it will be possible to implement the longitudinal polarization of the electron beam in order to measure the polarization asymmetry with high precision. One might hope to achieve here a precision in v_e/a_e of $\sim 10^{-3}$, corresponding to an error in $\sin^2\theta_w$

of 2.5×10^{-4}. Together, the accurate W^- mass measurement, the polarization asymmetry, and the improved precision in the cross-section and partial-width measurements will represent a new level of sensitivity to possible new phenomena in the electroweak sector.

Here we have mentioned only the expected impact of the planned LEP improvements on the electroweak theory. Of course the increased luminosity and energy will also open up new possibilities in the areas of particle searches and B physics.

Acknowledgments

It is a pleasure to thank all members of the four LEP experiments for making their results available for this review. In particular we wish to thank Drs. Ugo Amaldi, Edward Blucher, Albrecht Böhm, Marcello Mannelli, Manel Martinez, Aldo Michelini and David Stickland for their generous collaboration.

REFERENCES

[1] S.L. Glashow, Nucl. Phys. **B22** (1961) 579.
S. Weinberg, Phys. Rev. Lett. **19** (1967) 1264.
A. Salam, in Proc. 8th Nobel Symposium, p. 367, ed. N. Svartholm (Almqvist and Wiksell, Stockholm, 1968).
S.L. Glashow, J. Iliopoulos and L. Maiani, Phys. Rev. **D2** (1970) 1285.
G. 't Hooft, Nucl. Phys. **B33** (1971) 173 and **B35** (1971) 167.
G. Passarino and M. Veltman, Nucl. Phys. **B160** (1979) 151.

[2] F.J. Hasert et al., Phys. Lett. **46B** (1973) 138.

[3] B. Richter, Nucl. Instrum. Methods **136** (1976) 47.

[4] G. Arnison et al. (UA1 Collab.), Phys. Lett. **122B** (1983) 103.
M. Banner et al. (UA2 Collab.), Phys. Lett. **122B** (1983) 476.
G. Arnison et al. (UA1 Collab.), Phys. Lett. **126B** (1983) 398.
P. Bagnaia et al. (UA2 Collab.), Phys. Lett. **129B** (1983) 130.

[5] D. Decamp et al., Nucl. Instrum. Methods **A294** (1990) 121.

[6] P. Aarnio et al. (DELPHI Collab.), CERN-PPE/90-128, submitted to Nucl. Instrum. Methods.

[7] B. Adeva et al. (L3 Collab.), Nucl. Instrum. Methods **A289** (1990) 35.

[8] K. Ahmet et al. (OPAL Collab.), CERN-PPE/90-114, submitted to Nucl. Instrum. Methods.

[9] M. Greco, G. Pancheri-Srivastava and Y. Srivastava, Nucl. Phys. **B171** (1980) 118.
E.A. Kuraev and V.S. Fadin, Sov. J. Nucl. Phys. **41** (1985) 466.
G. Altarelli and G. Martinelli, in 'Physics at LEP', eds. J. Ellis and R. Peccei (Report CERN 86-02, Geneva, 1986), p. 46.
F.A. Berends, G. Burgers and W.L. van Neerven, Nucl. Phys. **B297** (1988) 429.

[10] G. Altarelli, R. Kleiss and C. Verzegnassi (eds.), Z physics at LEP 1 (CERN 89–08, Geneva, 1989), vol. 1, in particular the contributions of:
M. Consoli and W. Hollik, p. 7–54; G. Burgers and F. Jegerlehner, p. 55–88;
D. Bardin et al., p. 8^c-128.

[11] W.A. Bardeen et al., Phys. Rev. **D18** (1978) 3998.
K.G. Chetyrkin et al., Phys. Lett. **B85** (1979) 277.
M. Dine and J. Sapirstein, Phys. Rev. Lett. **43** (1979) 668.
W. Celemaster and R.J. Gonsalves, Phys. Rev. Lett. **44** (1979) 560; Phys. Rev. **D21** (1980) 3112.

[12] B.W. Lynn and R.G. Stuart, Nucl. Phys. **B253** (1985) 216.
A. Borelli, M. Consoli, L. Maiani and R. Sisto, Nucl. Phys. **B333** (1990) 357.
F.A. Berends, G. Burgers, W. Hollik and W.L. van Neerven, Phys. Lett. **203B** (1988) 177.

[13] G. Altarelli, R. Kleiss and C. Verzegnassi (eds.), Z physics at LEP 1 (CERN 89–08, Geneva, 1989), vol. 3.

[14] M. Böhm, A. Denner and W. Hollik, Nucl. Phys. **B304** (1988) 687.
F.A. Berends, R. Kleiss and W. Hollik, Nucl. Phys. **B304** (1988) 712.
H. Burkhardt, F. Jegerlehner, G. Penso and C. Verzegnassi, Z. Phys. **C43** (1989) 497.
S. Jadach et al., preprint CERN TH. 5888/90, submitted to Phys. Lett.

[15] W. Beenakker, F.A. Berends and S.C. van der Marck, Small-angle Bhabha scattering, Preprint-90-0695, Leiden Univ. (1990), submitted to Nucl. Phys. B.

[16] R. Bailey et al., LEP energy calibration, CERN–SL/90–95 (1990).
V. Hatton et al., LEP absolute energy in 1990, LEP Performance Note 12, Dec. 1990.

[17] Preliminary numbers as presented at the Aspen Winter Conference on Elementary Particle Physics, Aspen, Colo., 1991, and in the following internal notes:
OPAL Physics Note 90–21, 1990.
DELPHI Note 90–62 PHYS 80, 1990.

[18] ALEPH Collab.: D. Decamp et al., Phys. Lett. **231B** (1989) 519, **234B** (1990) 399, **235B** (1990) 399, and Z. Phys. **C48** (1990) 365.
DELPHI Collab.: P. Aarnio et al., Phys. Lett. **231B** (1989) 539 and **241B** (1990) 425, and P. Abreu et al., Phys. Lett. **241B** (1990) 435, preprint CERN–PPE/90–119 (1990).
L3 Collab.: B. Adeva et al., Phys. Lett. **231B** (1990) 509, **236B** (1990) 109, **237B** (1990) 136, **238B** (1990) 122, **247B** (1990) 173, **249B** (1990) 341 and **250B** (1990) 183.
OPAL Collab.: M.Z. Akrawy et al., Phys. Lett. **231B** (1989) 530, **235B** (1990) 379, **240B** (1990) 497 and **247B** (1990) 458.

[19] Computer program ZFITTER/ZBIZON: D. Bardin et al. (Dubna–Zeuthen radiative correction group), Z. Phys. **C44** (1989) 493 and Comp. Phys. Commun. **59** (1990) 303.
Computer program ZAPP: F.A. Berends, G. Burgers and W.L. van Neerven, Nucl. Phys. **B297** (1988) 429 and **B304** (1988) 921.
Computer Program MIZA: M. Martinez et al., preprint CERN–PPE/90–109, submitted to Z. Phys.

[20] ALEPH Collab., 'A measurement of the $Z \to b\bar{b}$ forward-backward asymmetry', presented at Aspen Conf. (see Ref. [17]).
B. Adeva et al. (L3 Collab), Phys. Lett. **252B** (1990) 713
[21] ALEPH Collab., 'Measurement of charge asymmetry in hadronic Z decays', submitted to Phys. Lett.
[22] ALEPH Collab., 'Measurement of τ polarization', presented at Aspen Conf. (see Ref. [17]).
[23] W. Beenakker, F.A. Berends and S.C. van der Marck, Nucl. Phys. **B349** (1991) 323.
[24] D. Decamp et al. (ALEPH Collab.), preprint CERN-PPE/90-194, submitted to Phys. Lett. B.
B. Adeva et al. (L3 Collab.), Phys. Lett. **252B** (1990) 703.
[25] J. Alitti et al. (UA2 Collab.), Phys. Lett. **241B** (1990) 150.
[26] F. Abe et al. (CDF Collab.), Phys. Rev. Lett. **63** (1989) 720.
[27] G.S. Abrams et al. (Mark 2 Collab.), Phys. Rev. Lett. **63** (1989) 2173.
[28] D. Decamp et al. (ALEPH Collab.), Phys. Lett. **246B** (1990) 306.
P. Abreu et al. (DELPHI Collab.), preprint CERN-PPE/90-163 (1990).
B. Adeva et al. (L3 Collab.), Phys. Lett. **248B** (1990) 203.
M.Z. Akrawy et al. (OPAL Collab.), CERN-PPE/90-150, submitted to Phys. Lett.
[29] F. Abe et al. (CDF Collab.), Phys. Rev. Lett. **65** (1990) 2243.
J. Alitti et al. (UA2 Collab.), Phys. Lett. **241B** (1990) 150.
[30] CDHS Collab.: H. Abramowicz et al., Phys. Lett. **57** (1986) 298 and A. Blondel et al., Z. Phys. **C45** (1990) 361.
CHARM Collab.: J.V. Allaby et al., Phys. Lett. **177B** (1986) 446 and Z. Phys. **C36** (1987) 611.
[31] F. Abe et al. (CDF Collab.), Argonne preprint ANL-HEP-PR- 90-109, submitted to Phys. Rev. D.

Imprimé au CERN. Prix : 0.90 Fr.